International Journal of Science and Engineering Applications
Volume 3 Issue 5, 2014, ISSN-2319-7560 (Online)

A Literature Review on Synthesis and Characterization of enamelled copper wire filled with CNT

D. Edison Selvaraj
Department of EEE
Panimalar Engineering College
Chennai, India

G. Dhivya
Applied Electronics
Dhanalakshmi Srinivasan
College of Engineering and
Technology Chennai, India

C. Pugazhendhi Sugumaran
Division of High Voltage
Engineering
College of Engineering
Guindy, Chennai, India

D. Krishnamoorthi
M. Raj Kumar
Department of EEE
Dhanalakshmi Srinivasan
College of Engineering and
Technology Chennai, India

M. Rajmal Joshi
Department of EEE
Panimalar Engineering College
Chennai, India

J. Ganesan
Department of EEE
Sree Sowdambika College of
Engineering, Aruppukottai,
India

S. Geethadevi
Department of EEE
Aurora Technological
and Research Institute, Uppal
Hyderabad, India

S. Dinesh Kumar
Department of EEE
St. Peter's University, Avadi,
Chennai, India

Abstract: This paper discusses about the survey on the various magazines, conference papers and journals for understanding the properties of enamelled copper wires mixed with nano fillers, fundamental methods for synthesis and characterization of carbon nanotubes. From all these papers, it was noted that the research work carried out in an enamelled copper wires filled with nano fillers has shown better results. It was also recorded that the research work was carried mostly with single metal catalysts and very little amount of research work has been carried out on the synthesis of carbon nanotubes using bimetallic catalysts.

Keywords: Enamel, Nano fillers, CNT, Al_2O_3, TiO_2

1. ENAMELLED COPPER WIRES FILLED WITH NANOFILLERS

P.C.Irwin, Y.Cao, A.Bansal and L.S.Schadler (IEEE 2003) explain the effects of nano-sized fillers on the thermal, mechanical and electrical properties of polymeric systems. Nanofilled polyimide films have shown increased elongation and strength to failure increased scratch hardness and increased thermal conductivity as compared to unfilled materials. Further testing is underway to determine the exact mechanism responsible for the improvement in thermal and mechanical properties [1].

J.Keith Nelson, John C.Fothergill, L.A.Dissado and W.Peasgood (IEEE 2002) examines the effects of nanofillers on space charge accumulation. The fundamental for controlling the dielectric strength of insulating polymers is the cohesive energy density and the associated free volume of the polymer structure are found by change in electric strength and glass transition temperature. Nanometric dimensions affect the dielectric properties. The interaction zone is responsible for the material property modifications [2].

Naoki Hayakawa and Hitoshi Okubo (IEEE 2008) determine the partial discharge characteristics of magnet wires. PD resistant enameled wire filled with inorganic materials has been developed to have longer breakdown lifetimes than those of conventional enameled wires. The breakdown lifetime characteristics of nanocomposite enameled wires increased as a function of nanofiller content. The PD resistance increased with the increasing nanofiller concentration [3]. K.Inuzuka, H.Inano, N.Hayakawa, T.Hirose, M.Hamaguchi and H.Okubo (IEEE 2006) measures the residual life of wires and surface roughness by scanning electron microscope. Nanofillers are useful for improving discharge resistance, matching of coefficient of thermal expansion, thermal conductivity, mechanical reinforcement and abrasion resistance. Increase in the loading weight of nanofiller cause an increase in partial discharge resistance but cause a reduction in mechanical strength which will lead to electrical degradation [4].

Santanu Singha and M.Joy Thomas (IEEE 2008) report an experimental work on the trends of dielectric permittivities and tan δ of epoxy nanocomposites with single nanofillers of Al_2O_3 and TiO_2 at lower filler concentrations (0.1%, 0.5%, 1% and 5%) over a frequency range of 1 MHz – 1 GHz. This shows that there is a strong dependence of the filler concentration and nanofiller permittivity at all these frequencies. Tanδ values in nano composites with Al_2O_3 fillers are found to be lower at all filler concentrations when compared with the value for unfilled epoxy [5].

Toshikatsu Tanaka, Masahiro Kozako, Norikazu Fuse and Yoshimichi ohki (IEEE 2005) gives a working hypothesis for

interaction zones. Several parameters such as chain mobility, chain conformation, crystallinity, degree of the stoichiometry are discussed to formulate the multi-cored model. Triboelectricity was considered for analysis of characteristics. Partial discharge takes zigzag paths to select weak regions consisting of polyamide matrices resulting in strong PD resistance [6].

Hulya Kirkici, Mert Serkan and K. Koppisetty (IEEE 2005) discuss the recent developments in the area of nano-dielectric materials. The effect of nano-scale fillers on electrical, thermal and mechanical properties of polymeric materials was observed. Nano composite materials have higher electrical breakdown strength [7].

M.Q.Nguyen, D.Malec, D.Mary, P.Werynswki, B.Gornicka, L.Therese and Ph.Guillot (IEEE 2009) compare the dielectric and mechanical properties of standard nanoscale -filled and micro scale filled varnishes. The PD occurring between consecutive turns was avoided by using corona-resistant wires and standard enameled wires with a corona-resistant varnish [8].

J. Keith Nelson and John C Fothergill show that the use of nano metric particles results in a substantial change in the behaviour of the composite, which can be traced to the mitigation of internal charge. Interaction zone is responsible for the material property modifications [9].

W. Pfeiffer and M. Paede show that the lifetime of insulation was affected by the environmental conditions. There is just a small dependency of the partial discharge characteristics on temperature and humidity [10].

2. SYNTHESIS AND CHARACTERIZATION OF CARBON NANOTUBE

2.1 Catalyst Preparation

The Biro L.P, Z.E.Horvath, A.A.Koos, Z.Osvath, Z.Vertesy and L.Tapazto, (2003) has suggested a mechanism for the growth of Carbon Nanotubes. Study on the morphology of the carbon structures grown by CVD showed a significant influence of temperature and the catalyst material on the quality of the carbon nanostructures was observed. The diameter of the nanotubes and the density is adjustable by choosing the corresponding temperature and/or the concentration of the catalyst solution [14].

Resasco. D.E, Alvarez W.E, F.Pompeo, L.Balzano and A.Borgna (2002) put forth a macroscopic characterization method involving surface area measurements and chemical analysis to compare the different nanotube specimens. An increase in the transition metal content of the catalyst yields more carbon nanotubes (up to a metal content of 10.0 wt %), but causes a decrease in carbon quality. The best compromise is to use 6.7 wt% of metal in the catalyst. Co gives superior results with respect to both the quantity and quality of the nanotubes. In the case of Fe, the quality is notably hampered by the formation of Fe3C particles [28].

Carole E. Baddour and Cedric Briens (2005) have proposed a paper reviewing the various plasma sources currently used in CNT growth, catalyst preparation and growth results. Since the technology is in its early stages, there is a general lack of understanding of growth mechanisms, the role of the plasma itself, and the identity of key species responsible for growth [15].

Li Y.,.Zhang X.B,.Tao X.Y, J.M.Xu, F.Liu and H.J.Geise (2005) has discussed that the decomposition of carbon precursors lead to the formation of a saturated carbon–metal solution. That is the common starting point for most growth models. The next stage of tube growth is carbon precipitation and graphite layer formation. Supersaturated conditions may be reached in different parts of a large flat metal particle independently and a few graphite islands can begin to grow. Further evolution depends on the initial cluster distribution, mobility of the graphite layers, precipitation rate, and possible surface distortions [25].

Jing Kong, Alan M.Cassell and Hongjie Dai (1998) has studied the growth of carbon species over metal catalyst particles under identical conditions. Smaller MWNTs are grown preferentially in narrower diameter distributions when the catalyst particle sizes are smaller. Taken together with the tip-growth and extrusion mechanisms that are well understood for the growth of filamentous carbon fibers, these results bring us closer to achieving structural control over nanotubes synthesized via CVD [22].

2.2 Characterization of Carbon nanotubes

From Li T.X., H.G. Zhang, F.J. Wang, Z. Chen and K. Saito (2007) showed that the size of the catalyst nanoparticles is the determining factor for the diameter of the CNT grown on it. Beyond this size correlation, only small nanoparticles are able to catalyze formation of CNT. This can be explained on one hand by the fact that such very small nanoparticles can exhibit peculiar electronic properties due to the unusual high ratio surface atom/bulk atom and on the other hand with a growth mechanism implying the formation of a carbon cap on the nanoparticle surface to reduce its unusual high surface energy. Finally, the crystallographic orientation of the catalyst nanoparticle can be crucial for CNT growth [24].

Liu B.C., B. Yu and M.X. Zhang (2005) proved that vertically well-aligned multi-walled carbon nanotubes (MWNTs) with uniform diameters (15 nm) were grown on catalytic probes at high yield rates in an inverse diffusion flame (IDF) of a co-flow jet configuration using methane as fuel. Varied parameters investigated included: alloy composition (e.g. Fe, Ni / Cu, Ni /Cr /Fe), sampling positions within the flame structure, and voltage bias applied to the probe substrate. Spontaneous Raman spectroscopy was utilized to determine the local gas-phase temperature, as well as the concentrations of carbon-based precursor species (e.g. CO, C_2H_2) within the flame structure at specific locations of carbon nanotube (CNT) growth during synthesis. The variation of the aforementioned parameters strongly affects CNT formation, diameter, growth rate, and morphology [23].

Matthieu Paillet, Jannik C.Meyer, Thiery Michel, Bruno Chaudret and Ahmed Zahab (2006) discussed the experimental and theoretical facts relevant for the catalytic growth of multiwall nanotubes by chemical vapor deposition, taking them as a basis for a more macroscopic, thermo dynamical model. It was found that the growth is mainly driven by a concentration gradient as opposed to a thermal

gradient, while the process temperature plays a key role in terms of activating diffusion [27].

Mariano Escobar, M. Sergio Moreno, Roberto J. Candal, M. Claudia Marchi, Alvaro Caso, Pablo I. Polosecki, Gerardo H. Rubiolo and Silvia Goyanes (2007) researched the rate of deposition of Carbon Nanotubes, their purity and wall thickness employing different Chemical Vapour Deposition processes. It was found that product purity and wall thickness was depended on process temperature, carbon precursor, concentration of catalyst during deposition [26].

Segura R., M.Flores, S.Hevia and P.Haberle (2007) investigated the Iron/molybdenum/magnesium mixed oxide prepared by a sol–gel method showing its high efficiency for synthesis of MWNTs through catalytic decomposition of Methane using Chemical Vapor Deposition method at 1000° C. The weight production of the as-grown MWNTs can reach as high as 30 times of the catalyst in 30 min growth. Upon SEM and TEM observations, the product is found to be compacted bundles of MWNTs. Microstructure of the tubes was characterized by Transmission Electron Microscopy and Raman Spectroscopy. Thermal gravimetric analysis examination showed that the content of MWNT is high. Using this high-efficient catalyst, the cost of producing carbon nanotubes can be greatly reduced [29].

Yu G.J., Gong J.L, S.X. He, J.Q. Cao and Z.Y. Zhu (2006) demonstrated that uniform iron-molybdenum nanoparticles can be prepared by thermal decomposition of metal carbonyl complexes using a mixture of long-chain carboxylic acid and long-chain amine as protective agents. The sizes of the nanoparticles can be systematically varied from 3 to 14 nm by changing the experimental conditions. High-resolution TEM images and EDX data show that the prepared nanoparticles are highly crystalline iron nanoparticles containing 4% molybdenum. The effects of the concentration, reaction time, the ratio of metal carbonyl complexes versus protective agents, and the ratio of acid/amine of the protective agents on the sizes of the produced nanoparticles were systematically studied. The prepared nanoparticles were used as catalysts for single-walled carbon nanotube growth and the results indicate that there is an upper limit for the size of the catalyst particles to nucleate single walled carbon nanotubes [32].

2.3 Synthesis of carbon nanotubes by CVD

Carbon Guo. P.S. Z. Sun, Y.W. Chen and Z.H. Zheng (2006) has conducted a research using nickel foil as both substrate and catalyst, reported a simple, cheap and easily controllable thermal chemical vapor deposition (CVD) for mass synthesis of carbon nanotubes (MWNTs). Grams of CNTs with high purity and good uniformity have been obtained on the nickel foil at 550 °C in a gas mixture of C_2H_2 and H_2. The as-prepared CNTs were screen-printed on Ag electrodes patterned on glass to form field emission cathodes. The cathodes exhibit excellent field emission properties, with a turn-on field of 1.0 V/μm, the emission current density of 1 mA/cm^2 at 2.5 V/μm, and uniform emission luminescence. This CVD method shows great promise in large-scale production of raw materials of CNTs for application of field emission display [19].

Andrews R., D.Jacques, E.C.Dickey and D.Qian (2003) showed that Chemical vapor deposition (CVD) is the most promising synthesis route for economically producing large quantities of carbon nanotubes. We have developed a low-cost CVD process for the continuous production of aligned multiwall carbon nanotubes (MWNTs). The effects of reactor temperature, reaction time, and carbon partial pressure on the yield, purity, and size of the MWNTs produced were reported. A simple method for purifying and healing structural defects in the nanotubes is described. The dispersion of nanotubes in polymer matrices has been investigated as a means of deriving new and advanced engineering materials. These composite materials have been formed into fibers and thin films and their mechanical and electrical properties determined [13].

Sing B.K, Sung-Wook Cho, K.S.Bartwal, Nguyen Duc Hoa and Hojin Ryu (2007) proved that Multiwalled carbon nanotubes (MWNTs) can be synthesized by chemical vapor deposition technique using MgO supported bimetallic Fe–Mo catalyst. The role of Mo on the quality of as-synthesized CNTs and their application in field emission has been investigated. The field emission properties of the device fabricated from the CNTs synthesized with Fe–Mo catalyst was found to be better than the similar device prepared with CNTs synthesized with Fe catalyst alone [30].

Tao X.Y. a,b, X.B. Zhang a,b,., F.Y. Sun c, J.P. Cheng a,b, F. Liu a and Z.Q. Luo (2007) conducted an experimental study to investigate the synthesis of multi-walled carbon nanotubes (CNTs) in counter flow methane–air diffusion flames, with emphasis on effects of catalyst, temperature, and the air-side strain rate of the CNT growth. The counter flow flame was formed by fuel (CH4 or CH4+N2) and air streams impinging on each other. Two types of substrates were used to deposit CNTs. Ni-alloy (60% Ni + 26% Cr + 14% Fe) wire substrates synthesized curved and entangled CNTs, which have both straight and bamboo-like structures; Si-substrates with porous anodic aluminum oxide (AAO) nanotemplates synthesized well-aligned, self-assembled CNTs thermocouple with a 0.3 mm bead junction. It was found that temperature could affect not only the success of CNTs synthesis, but also the morphology of synthesized CNTs. It was also found, against previous general belief, that there was a common temperature region (1023–1073 K) in chemical vapor deposition (CVD) where CNTs could be produced [31].

3. CONCLUSION

From the literature survey it was observed that the research work carried out in an enamelled copper wire filled with nano fillers has shown better results. It was also noted that the research work was carried mostly with single metal catalysts and very little amount of research work has been carried out on the synthesis of carbon nano tubes using bimetallic catalysts. Hence it was decided to take up research on synthesis of carbon nanotubes using bimetallic catalyst. nanotubes [32].

4. REFERENCES

[1] P.C.Irwin, Y.Cao, A.Bansal and L.S.Schadler , “Thermal and mechanical properties of polyimide nanocomposites”, IEEE 2003.

[2] J.Keith Nelson, John C.Fothergill,L.A.Dissado and W.Peasgood, “Towards an understanding of nanometric dielectrics”, IEEE 2002.

[3] Naoki Hayakawa and Hitoshi Okubo, "lifetime characteristics of nanocomposite enameled wire under surge voltage application", IEEE 2008.

[4] K.Inuzuka, H.Inano, N.Hayakawa, T.Hirose, M.Hamaguchi and H.Okubo , "Partial discharge characteristics of nanocomposite enameled wire for inverter fed motor", IEEEE 2006.

[5] Santanu Singha and M.Joy Thomas, "Permittivity and tan delta characteristics of epoxy nanocomposites in the frequency range of 1 mhz – 1 ghz", IEEE 2008.

[6] Toshikatsu Tanaka, Masahiro Kozako, Norikazu Fuse and Yoshimichi ohki, "Proposal of a multi-cored model for polymer nanocomposite dielectrics", IEEE 2005.

[7] Hulya Kirkici, Mert Serkan and K.Koppisetty , "Nano-dielectric materials in electrical insulation application", IEEE 2005.

[8] M.Q.Nguyen ,D.Malec ,D.Mary ,P.Werynswki ,B.Gornicka, L.Therese and Ph.Guillot, "Investigations on dielectric properties of enameled wires with nanofilled varnish for rotating machines fed by inverters", IEEE 2009.

[9] J. Keith Nelson and John C Fothergill, "Internal charge behaviour of nanocomposites", Institute of Physics Publishing, 2004.

[10] W. Pfeiffer and M. Paede, "About the influence of the environmental conditions on the partial discharge characteristics of enameled wire at high frequency voltage".

[11] IEC 60851, Methods of test for winding wires, 1994.

[12] IEC 61251: Electrical insulating materials – A.C. voltage endurance evaluation. IEC, Geneva, 1993.

[13] Andrews R., D.Jacques, E.C.Dickey and D.Qian,(2003) "Synthesis and growth mechanism of multiwalled carbon nanotubes", Center for Applied Energy Research, University of Kentucky.

[14] Biro L.P., Z.E.Horvath, A.A.Koos, Z.Osvath, Z.Vertesy and L.Tapazto, (2003) "Direct synthesis of multi-walled and single walled carbon nanotubes by spray-pyrolysis", Journal of Optoelectronics and advanced materials, Vol.5, issue 3, pp 661- 666.

[15] Carole E. Baddour and Cedric Briens (2005) "Carbon Nanotube Synthesis: A Review", International Journal of Chemical Reactor Engineering, Vol 3, Review R3

[16] Couteau E., J.W. Seo , L Thien-Nga , Cs. Mik , R.Gaal , L.Forro, (2003) "CVD synthesis of high-purity multiwalled carbon nanotubes using CaCO3 catalyst support for large-scale production" Chemical Physics Letters 378, pp 9–17.

[17] Engel-Herbert R. a, H. Pforte b, T. Hesjedal, (2007) "CVD synthesis and purification of single-walled carbon nanotubes using silica-supported metal catalyst" Materials Letters 61, pp 2589–2593.

[18] Giuseppe Gulino, Ricardo Vieira, Julien Amadou, Patrick Nguyen, Marc J. Ledoux, Signorino Galvagno, Gabriele Centi, Cuong Pham- Huu,(2005) "C2H6 as an active carbon source for a large scale synthesis of carbon nanotubes by chemical vapour deposition" Applied Catalysis A:General 279, pp 89–97.

[19] Guo. P.S. Z. Sun, Y.W. Chen, Z.H. Zheng (2006) "A novel approach to mass synthesis of raw CNTs for printed field emission cathodes by chemical vapour deposition" Materials Letter, Vol.60, pp 966-969.

[20] Hiroshi Kinoshita ., Ippei Ippei, Hirokazu Sakai, Nobuo Ohmae,(2007) "Synthesis and mechanical properties of carbon nanotube/diamond-like carbon composite films", Diamond & Related Materials 16, pp 1940–1944.

[21] Jipeng Cheng, Xiaobin Zhang , Zhiqiang Luo, Fu Liu, Ying Ye , Wanzhong Yin , Wei Liu , Yuexin Han, (2006) "Carbon nanotube synthesis and parametric study using $CaCO_3$ nanocrystals as catalyst support by CVD" Materials Chemistry and Physics 95, pp 5–11

[22] Jing Kong, Alan M.Cassell, Hongjie Dai,(1998) "Chemical Vapour Deposition of methane for single walled carbon nanotubes", Chemical Physics Letters 292,pp 567 – 574.

[23] Liu B.C., B. Yu, M.X. Zhang , (2005)"Catalytic CVD synthesis of double-walled carbon nanotubes with a narrow distribution of diameters over Fe–Co/MgO catalyst" Chemical Physics Letters 407, pp 232–235.

[24] Li T.X., H.G. Zhang , F.J. Wang, Z. Chen , K. Saito, (2007) "Synthesis of carbon nanotubes on Ni-alloy and Si-substrates using counter flow methane air diffusion flames", Proceedings of the Combustion Institute 31, pp 1849–1856

[25] Li Y.,.Zhang X.B,.Tao X.Y, J.M.Xu, F.Liu and H.J.Geise, (2005) "Single phase MgMoO4 as catalyst for the synthesis of bundled multi-wall carbon nanotubes by CVD", Journal of Carbon, 43, pp 1325 – 1328.

[26] Mariano Escobar, M. Sergio Moreno, Roberto J. Candal, M. Claudia Marchi, Alvaro Caso, Pablo I. Polosecki, Gerardo H. Rubiolo, Silvia Goyanes,(2007) "Synthesis of carbon nanotubes by CVD: Effect of acetylene pressure on nanotubes characteristics" Applied Surface Science 254, pp 251 -256

[27] Matthieu Paillet, Jannik C.Meyer, Thiery Michel, Bruno Chaudret and Ahmed Zahab, (2006) "Selective growth of large chiral angle single walled carbon nanotubes", Diamond & Related Materials, 15, pp 1019 – 1022

[28] Resasco. D.E., Alvarez W.E., F.Pompeo, L.Balzano and A.Borgna, (2002) "A scalable process for production of single-walled carbon nanotubes by catalytic disproportionation of CO on a solid catalyst", Journal of Nanoparticle Research, Vol 4, pp 131 – 136.

[29] Segura R., M.Flores, S.Hevia, P.Haberle, (2007) "Synthesis, characterization and spectroscopy of carbon based nanoscale materials", Microelectronics Journal Article in press.

[30] Sing B.K, Sung-Wook Cho, K.S.Bartwal, Nguyen Duc Hoa,Hojin Ryu(2007) "Synthesis of MWNTs using Fe–Mo bimetallic catalyst by CVD method for field emission application", Solid State Communications 144, pp 498–502.

[31] Tao X.Y. a,b, X.B. Zhang a,b,., F.Y. Sun c, J.P. Cheng a,b, F. Liu a, Z.Q. Luo,(2007) "Large-scale CVD synthesis of nitrogen-doped multi-walled carbon nanotubes with controllable nitrogen content on a CoxMg1-xMoO4 catalyst", Diamond & Related Materials 16, pp 425–430

[32] Yu G.J., Gong J.L, S.X. He, J.Q. Cao, Z.Y. Zhu, (2006) "Efficient synthesis of carbon nanotubes over rare earth zeolites by thermal chemical vapor deposition at low temperature" Diamond & Related Materials 15, pp 1261 – 1265

[33] M S Naidu and V Kamaraju, "High Voltage Engineering" Solid dielectrics used in practice pp 106 – 122.

[34] Dieter Kind and Hermann Kamer, "High Voltage Insulation Technology" 1985.

[35] E. Kuffel, W.S. Zaengl and J. Kuffel, "High Voltage Engineering Fundamentals" Partial discharge measurements pp 421 – 456.

[36] Partial discharge measurements, IEC 270, 1981.

[37] IEC standard 60270: 1999 Partial discharge measurements.

[38] B. Tareev "Physics of Dielectric Materials" Tests for thermal ageing pp 234 – 235.

[39] M. Arumugam "Material Science" Scanning Electron Microscope pp 423.

International Journal of Science and Engineering Applications
Volume 3 Issue 5, 2014, ISSN-2319-7560 (Online)

Design optimization of Floor Cranes

A. Balaji
Department of Mechatronics Engineering
Kongu Engineering College
Erode, India

H. Jahir Hussain
Department of Mechatronics Engineering
Kongu Engineering College
Erode, India

M.R. Faheem Ashkar
Department of Mechatronics Engineering
Kongu Engineering College
Erode, India

Abstract: This paper inculcates a way to make the floor crane as more efficient with less material requirement. This has been achieved by minimizing reach of the crane from the floor. The crane is assumed to be cantilever type. Also tension and acceleration in steel ropes are analysed to ensure the safety. The optimized crane successfully passed the various analysing tests which include deflection, bending moment, rope tension and acceleration of the loads in the rope. It also includes another method which provides the virtual user interface for the design engineer. By providing the crane dimensions in the virtual panel, the predefined program automatically creates the CAD modelling in the CAD software. The program is made with visual studio and Solid works macro. Finally, this work reduces the burden on the design engineer and increases the productivity.

Keywords: cranes; floor cranes; optimization; virtual CAD model; solid works

1. INTRODUCTION

A crane is a machine which is used in material handling processes. It is used to lift, lower and move any materials horizontally[1]. Cranes are used in construction, transportation, and manufacturing sections. It uses one or more simple machines to create mechanical advantage and thus move loads beyond the normal capability of a human[2]. Floor crane is taken into consideration in this work.

2. PROBLEM STATEMENT

Floor crane is shown in Figure 1 which has two columns for length 1m and 1.2m. The design separates the two columns with the distance of 0.6m. The horizontal beam for about 1.5m is defined as reach of the crane and it supports the rope. The whole crane is fixed at the base and the counter weight is loaded at the back. The problem is within the distance 0.6m, the design shoots up the length for about 0.2m. Hence the whole crane is modelled and analysed for deflection. The result shows that the deflection at the second column is very high.

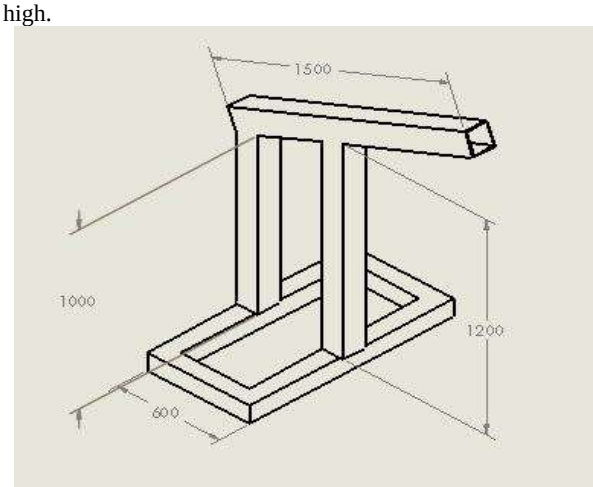

Figure 1 CAD model of floor crane

3. VIRTUL CAD MODELING

Floor crane design varies with capacity and reach of the crane. Depending on the reach, the length of the horizontal beam is varied. Hence, for every time the designer has to design the whole crane. In order to eliminate this problem, virtual CAD modeling[3] is proposed. Designer can modify the solid works macro in Microsoft visual basic, Microsoft visual studio for applications to fit the need.

4. DESIGN OPTIMIZATION OF FLOOR CRANE

In order to rectify the problem, the second column length is reduced from 1.2 meter to 1 meter. By doing so, the reach of the crane from the floor is reduced from 830mm to 780mm and angle of the rope beam is reduced from 22.2 degree to 10.8 degree. This final optimized design is analysed under various conditions to determine whether the design is safe and efficient in comparison with the previous design. Figure 2 shows the existing and optimized design of floor crane.

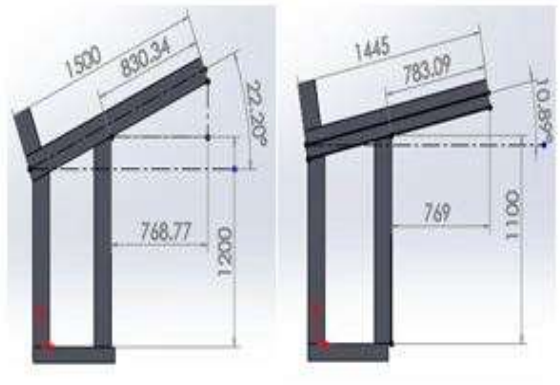

Figure 2 Existing and Optimized design of crane

5. DESIGN ANALYSIS

5.1 Bending Moment

The column 1 and column 2 is rigidly fixed with the floor. Hence the beam in which the work outside the floor is considered as cantilever beam and analyzed for bending moment. The Figure 3 shows the calculation of bending moment. From the calculation, the bending moment in the optimized design is reduced about 23620 N mm.

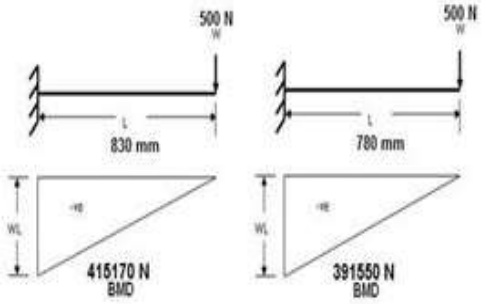

Figure 3 Bending moment calculation

5.2 Deflection

The deflection analysis of cantilever beam is analyzed which is shown in Figure 4. The material is Mild Steel and the details include young's modulus is 210GPa; Poisson's Ratio is 0.3 and density about 7.85 g/cm^3[4]. From the result shown in figure 4, the deflection of beam is reduced from 0.058mm to 0.032mm.

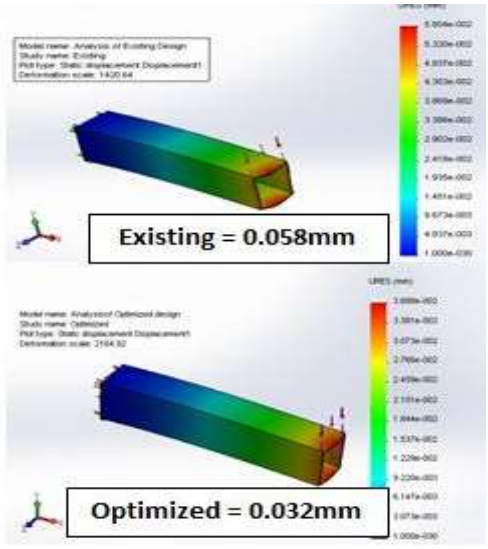

Figure 4 Deflection Analysis of Cantilever Beam

6. SAFETY ANALYSIS

6.1 Rope Tension Analysis

From the figure 2, the angle of the beam is changed from 22 degree to 10 degree. Based on the D' Alembert's principle, the tension and acceleration in the rope is calculated for sample loads. On resolving the forces in the figure 5, the tension and acceleration for the existing (angle = 22.2) is about 12N and 4.63 m/s^2 and for the optimized (angle = 10.89) is about 8.34N and 5.26 m/s^2 respectively.

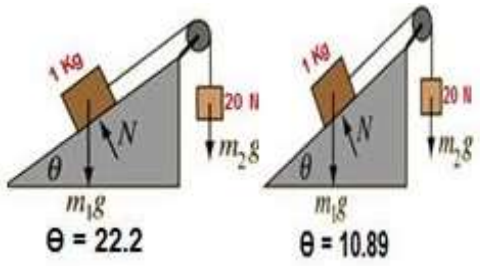

Figure 5 Force acting on different angles

Steel rope, used for lifting load, in the floor crane is modelled in Solid works and the sample tension is applied for the two different angles as shown in the figure 6. The rope used is 6*7 steel ropes with nominal diameter of 32mm. The result shows that deflection in the optimized angle is much lesser than the existing design.

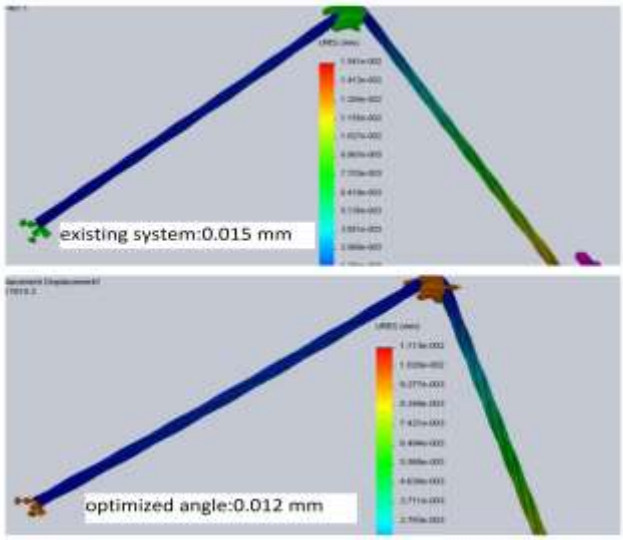

Figure 6 Rope Tension Analysis

6.2 Load with acceleration

From the rope tension analysis calculation, acceleration in the rope is also calculated. Hence, the load with acceleration is applied to both the existing and optimized design to check the deflection using Solid works simulation. The result as shown in figure 8 shows that the deflection in the optimized design is much lesser than the existing design. Figure 7 shows the applied initial acceleration in the rope.

Figure 7 Initial conditions in solid works

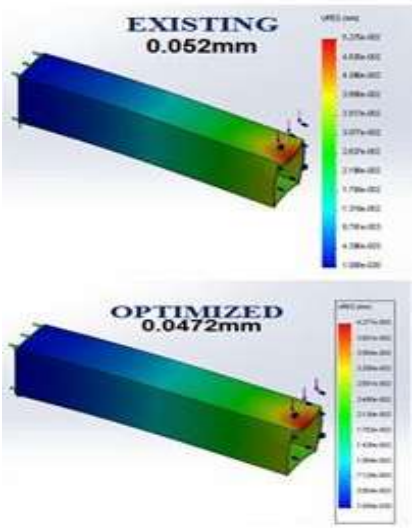

Figure 8 Deflection with acceleration analysis

7. RESULTS

The table 1 tabulates the advantage of optimized floor crane design over the existing one. Based on the analysis and results, the new optimized floor cane has been successfully fabricated which is shown in figure 9.

Table 1 Comparative Study

ANALYSIS	EXISTING	OPTIMIZED
Bending Moment	415170 Nmm	391550 Nmm
Deflection	0.0587 mm	0.0325 mm
Rope Tension	High	Low
Deflection with Acceleration	0.0527 mm	0.0427 mm
Material Requirement	More	Less

Figure 9 Optimized Floor Crane

8. CONCLUSIONS

[1] Crane would be safer (Rope tension is reduced)

[2] Crane would be stronger (Deflection and stress is reduced)

[3] Crane would be cheaper (Material requirement is reduced)

9. REFERENCE

[1] American Society of Mechanical Engineering (ASME), 'Electric Overhead Travelling Crane-Specifications and Details', Article 57, 2012

[2] American Society of Mechanical Engineering (ASME), 'Fixtures and loads for the Floor crane design', Article 72, 2010

[3] American Society of Mechanical Engineering (ASME), 'Steel Rope specifications and details', Article 57, 2012

[4] American Standard National Institute (ASNI), 'Types of Material Handling Cranes- overview', Article 63, 2008

[5] CAD sharp Journal, 'Solid works in Visual Studio', Article-13, 2011

[6] D. Saravanan, 'Solid works 2012 for Designers', 2nd Edition, Wiley India Publications

International Journal of Science and Engineering Applications
Volume 3 Issue 5, 2014, ISSN-2319-7560 (Online)

Short Notes for Understanding the Basics of Nano Technology

D. Edison Selvaraj
S. Sivaa Priyan
Department of EEE
Panimalar Engineering College
Chennai, India

C. Pugazhendhi Sugumaran
Division of High Voltage Engineering
College of Engineering
Guindy, Chennai, India

D. Krishnamoorthi
M. Raj Kumar
Department of EEE
Dhanalakshmi Srinivasan College of Engineering and Technology Chennai, India

M. Rajmal Joshi
Department of EEE
Panimalar Engineering College
Chennai, India

J. Ganesan
Department of EEE
Sree Sowdambika College of Engineering, Aruppukottai, India

S. Dinesh Kumar
Department of EEE
St. Peter's University, Avadi, Chennai, India

S. Geethadevi
Department of EEE
Aurora Technological and Research Institute, Uppal
Hyderabad, India

Abstract: In this paper, the basic terms and definitions of nano technology was discussed. The characteristics, advantages and disadvantages of nano technology were discussed. Applications of nano technology were also mentioned. This paper would be useful to young engineers to study the fundamentals of nano particles. Two approaches used for nano technology were also elaborated.

Keywords: Nano Technology, Advantages, Disadvantages, Applications, Quantum dots, Nano particles, Nano wires

1. INTRODUCTION

1.1 Definition of Nanotechnology

The definition of nano technology was given by National Nanotechnology Initiative in U.S. Nano technology deals with structures having particle size of 1 to 100nm [1-2]. Nanotechnology is the design, fabrication and use of nano structured systems and the growing, assembling of such systems mechanically, chemically or biologically to form nano scale systems and devices [3-4].

1.2 Characteristics of nano technology

1. It is very diverse.
2. It is based upon molecular self-assembly.
3. It is used in fields of science, organic chemistry, molecular biology, semiconductor physics, micro fabrication medicine, electronics & energy production.
4. It was used to create many new materials.
5. It has impact on environment and economics.
6. It is the engineering of functional systems at the molecular scale.
7. It is used to make high performance products.

1.3 Applications of nano technology

1. Nano capacitors based filters
2. Nano transformer based SMPS
3. Nano cables
4. Nano insulators
5. Nano powders used for welding rods and electrodes
6. Nano based rectifiers
7. Nano resistance
8. Nano engineering materials
9. Silicon steel mixed with 5% nano – magnetic properties
10. Nano sic Arrestors
11. Nano ZnO Arrestors
12. Nano technology used in receivers
13. Nano alloys
14. Nano capacitor based microphones
15. Nano electrets
16. Nano nuclear engineering
17. Nano thermo electric materials
18. Nano medicines

1.4 Limitation of nano Technology

1. Integration of nano structure and nano materials was not easy.
2. Demonstration of novel tools to study at nano meter was difficult.

3. New measurement technologies were more challenging than ever.
4. It requires extremely sensitive instrumentation.
5. Monitoring and manipulation of the material processing in the atomic level was crucial.
6. Self-purification of nano materials makes doping very difficult.
7. Huge surface energy.
8. Uniform size distribution was difficult to achieve in nano materials.
9. It is not easy to achieve desired size, morphology, Chemical composition and physical properties.
10. Ostwald ripening and agglomeration would occur.

1.5 Examples of nano particles

1. 1 nm = 10^{-9}m
2. Spacing between the atoms in carbon-carbon bond was 0.12 to 0.15 nm.
3. DNA double helix has a diameter of 2 nm.
4. Bacteria have a length of 200 nm.

1.6 Quantum size effect

The electronic properties of solids were altered with the reduction in particle size [5-6]. The physical, chemical, mechanical, electrical, thermal, magnetic & optical properties of solids were changed with the decrease in the particle size. This was called as quantum size effect.

Example: 1.Opaque substance become transparent copper
2. Stable materials turn combustible aluminum
3. Insoluble materials become soluble gold

2. MAIN APPROACHES IN NANO TECHNOLOGY

There are two main approaches in nano technology.
1. Bottom up approach.
2. Top down approach.

2.1 Bottom up approach

1. In the bottom approach, materials and devices were built from molecular components which assemble themselves chemically by principles molecular recognition.
2. It utilities the concept of molecular self-assembly and supra molecule chemistry to automatically arrange themselves into some useful conformation
3. It involves the concept of molecular recognition.
4. Molecules can be designed due to non-covalent intermolecular forces
5. In this process, nano phase materials are produced by building of atom by atom, molecule by molecule or cluster by cluster. This process was used to build larger objects from smaller buildings blocks
6. It is opposite of top-down approach.

2.1.1 Examples

1. Watson – Crick base pairing
2. Enzyme – substrate interactions
3. Pulsed laser deposition
4. Chemical vapour deposition
5. Colloidal dispersion
6. Nano lithography
7. Nano manipulation

2.1.2 Advantages

1. Two or more components can be designed to be complementary and mutually attractive to make a complex.
2. It is used to produce devices in parallel.
3. It is cheaper than top-down method.
4. It is difficult for complex assembly.
5. It is used to obtain nano structures with fewer defects
6. More homogeneous chemical composition
7. Long life
8. Less time
9. Reduction of Gibbs free energy
10. Allows smaller geometries
11. Easier
12. Economical
13. It doesn't waste material

2.1.3 Applications

1. Production of salt & nitrate
2. Growth of single crystal
3. Deposition of films
4. Fabrication of organic semi-conductors
5. Manufacture of carbon nano tubes and silicon nano wires

2.1.4 Disadvantages

There was no difference in the physical properties of materials depending upon the synthesis method. But, chemical composition, crystallinity and microstructure of the material can change due to kinetic reasons depending upon the synthesis method. Consequently, the physical properties can also change.

2.2 Top down approach

In the top down approach, nano objects were constructed from larger entities without atomic level control.

2.2.1 Examples

1. Attrition or milling
2. Etching
3. Emulsification
4. Comminution

2.2.2 Advantages

1. Stronger covalent bonds were created by this method.

2.2.3 Limitations

1. Imperfection of surface structure
2. Crystallographic damage
3. Not smooth
4. Contains lot of impurities & structural defects
5. Change in physical property & surface chemistry due to large surface over volume ratio.
6. Reduced conductivity due to inelastic surface scattering
7. Excessive heat due to surface defects
8. In this process, bulk materials are broken into smaller nano size particles
9. Advantages
10. Stronger covalent bonds are created by this method.

2.2.4 Applications

1. Synthesis of nano particles such as Al2O3, SiO2, ZrO2nano fillers used in enamel
2. It is used in the synthesis of nano fillers such as Al2O3, SiO2, ZrO2, TiO2 used in enamel.

3. CLASSIFICATION OF NANO PARTICLES

Nano particles were particles that would have dimension of 100 nm or less in size [7-8].

According to the shape of the crystallites nano materials were classified into four categories:

1. Clusters or powders (MD = 0)
2. Multi layers (MD = 1)
3. Ultrafine grained over layers or buried layers (MD = 2)
4. Nano materials composed of equiaxed nano meter sized grains (MD = 3)

Nano materials were classified according to their chemical composition as follows.

1. Materials with same chemical composition.
   Example:
   Semi crystalline polymers
   Multi layers of thin film crystallites separated by an amorphous layer
   Si: N: H
   Nc - si
2. Materials with different chemical composition of grains.
   Example:
   Quantum well structures.
3. Materials having different chemical composition of its forming mater including different interfaces.
   Example:
   Ceramic of alumina with Ga in its interface
4. Nano materials formed by nano metre sized grains dispersed in a matrix of different chemical composition.
   Example:
   Precipitation hardened alloys.
   Nano meter sized Ni-Al precipitates dispersed in a nickel matrix high temperature materials used in modern jet engines.
   Precipitation hardened Ni3Al/Ni alloys.

4. PROPERTIES OF NANO MATERIALS:

The properties of many conventional materials change when formed from nano particles [9-11]. This was due to the reason that nano particles have a greater surface area per weight than larger particles.

4.1 Physical properties

1. Large fraction of surface atoms.
2. Large surface energy.
3. Spatial confinement.
4. Reduced imperfections.
5. Lower melting point.
6. Lower phase transition temperature.
7. Reduced lattice constants due to a huge fraction of surface atoms.

4.2 Mechanical properties

The enhancement in mechanical strength was simply due to the reduced probability of defects.

1. Carbon nanotubes were the strongest and stiffest materials. This was due to covalent sp2 bonds formed between the individual carbon atoms.
2. Multi walled CNT have a tensile strength of 63GPA.Individual CNT have a strength up to 100GPA.
3. CNT has a low density of 1.3 to 1.4 g/cm3. Specific strength - 48,000 kNmKg-1
4. CNT undergo bucking when placed under compressive, torsion or bending stress due to it hollow structure and high aspect ratio.

4.3 Optical Properties

Optical properties of nano material can be significantly different from bulk crystals [10]. The optical absorption peak of a semi conductor nano particle shifts to a short wavelength due to an

increased band gap [12-13]. The optical absorption peak of metals was shifted by hundreds of nm. The colour of metallic nano particle may change with their sizes due to surface Plasmon resonance.

4.4 Electrical Properties

1. The dielectric strength of the insulating materials were improved by adding nano fillers of SiO2, TiO2, ZrO2, ZnO2 and so an.
2. The insulation resistance of the enamel was increased by adding nano fillers of SiO2, TiO2, ZrO2, ZnO and so an.
3. Dielectric loss, temperature rise was increased in the enamel by the addition of ZnO, Sic, ZrO2, TiO2, and SiO2 nano fillers.
4. The value of constant and capacitance was improved by the addition of nano fillers polyamide enamel used as the coating of the winding of the electrical machines.
5. The efficiency, thermal withstanding capacity of the electrical machines was improved by the addition of nano fillers to the enamel used for the coating of the windings of it.
6. Harmonics and EMI of the electrical machines were reduced by the addition of nano fillers to the enamel used for the coating of the windings of the electrical machines.
7. Electrical conductivity decreases with the reduction in dimension due to increased surface scattering particle charging energies were altered by hundreds of MV via particle size and safe.
8. Electrical conductivity of nano materials could be improved due to the better ordering in micro structure.

4.5 Magnetic Properties

Magnetic properties of nano materials were different from that of bulk materials. Ferromagnetism of bulk materials disappears and transfers to super paramagnetism in nano meter scale due to the huge surface energy. Iron oxide nano particles were used to improve MRI images of cancer tumours. The nano particles were coated with a peptide that binds to a cancer tumour. Once the nano particles were attached to the tumour, the magnetic property of the iron oxide enhances the images from the magnetic resonance imaginary scan.

4.6 Thermal Properties

Self purification was an intrinsic thermodynamic property of nano material Heat treatment increases the diffusion of impurities, intrinsic structural defects and dislocation. Increased perfection would have appreciable impact on the chemical and physical properties.

4.7 Chemical Properties

1. Chemical stability was improved.
2. Chemical properties were size dependent.
3. Chemical properties of nano materials were changed by adjusting the size, shape and extent of agglomeration.

5. NANO PARTICLES

Nano particles were particles that have particle size of 100 nm or less. The properties of many conventional materials change when formed from nano particles. This was due to the reason that nano particles have a greater surface area per weight than larger particles. Iron oxide nano particles were used to improve MRI images of cancer tumours. The nano particles were coated with a peptide that binds to a cancer tumour. Once the nano particles were attached to the tumour, the magnetic property of the iron oxide enhances the images from the magnetic resonance imagniary scan.

6. QUANTUM DOTS

1. A quantum dot was absorption of matter whose excitons were confined all three spatial dimensions.
2. They have electronic properties intermediate between bulk semiconductors and discrete molecules.
3. They were discovered at 1980 by Alexei E Kimov in a glass matrix and by Louis E. Brus in colloidal solutions.
4. The term “quantum dot” was coined by Mark Reed.
5. Quantum dots were observed in transistors, solar cells, LEDs and Diode lasers.
6. Quantum dots were stated as “Semiconductors whose electronic characteristic were closely related to the shape and size of the individual crystal.”

6.1 Characteristics of Quantum dots

1. Smaller crystal size.
2. Larger band gap.
3. Greater difference in energy between the highest valence band and lowest band.
4. More energy was needed to excite the dot.
5. High level of control over the size of the crystals.
6. Very precise control over the conductive properties of the material.
7. Quantum dots of different sizes can be assembled into a gradient multi layer nano film.
8. Colour shift in fluorescent dye applications.
9. Diameter of quantum dots was 10nm.

6.2 Production

Quantum wires, wells and dots were produced by different methods.

1. Advanced Epitaxial technique

(i) Molecular Beam epitaxy
(ii) Metal organic vapor phase epitaxy.
2. Chemical methods.
3. Ion implantation.
4. Lithography.
5. Colloidal synthesis.
6. Etching.
7. Quantum cryptography.
8. High temperature dual injection.

6.3 Colloidal Synthesis

Colloidal semiconductor nano crystals were synthesized from precursor compounds dissolved in solutions. The synthesis of colloidal quantum dots was based on a three component system composed of

1. Precursors.
2. Organic surfactants.
3. Solvents.

The precursors transforms into monomers while heating a reaction medium to high temperature. Once the monomers reach a super saturation level, the nano crystal growth starts with a nucleation process. Temperature was an important factor in determining the optimal conditions for the nano crystal growth.
Another important factor was the monomer concentration.
The growth of nano crystals could occur in two regimes:

1. Focusing
2. Defocusing

6.3.1 Focusing

At higher monomer concentrations, the crystal size is small, resulting in the growth of all particles. In this regime, smaller particles grow faster than large ones resulting in focusing of the size distribution to yield mono disperse particles.

6.3.2 Defocusing

When the monomer concentration was depleted during growth the critical size becomes larger than the average size present and the distribution 'defocuses' as a result of Ostwald ripening.
Quantum dots were made of allow such as

1. Cadmium selenide.
2. Cadmium sulfide
3. Indium arsenide.
4. Indium phosphide.
5. Cadmium selenide sulfide.

6.3.3 Advantages

1. Convenient method
2. Used for commercial application.
3. Least toxic.

6.4 Lithography and Etching

Quantum dots obtained by lithography and etching has a dimension of 100nm. It was used for semi conductor hetero structures. A lateral quantum dot was obtained by electron beam lithography.

6.5 Epitaxy

6.5.1 Types

1. Molecular beam epitaxy.
2. Metal organic vapour phase epitaxy.

Material was grown on a substrate. This growth is called as stranski - krastanov to form quantum dot.

6.5.2 Drawbacks

1. Costly.
2. Lack of control.

6.6 High Temperature Dual Injection

It is impossible for the manufacture for large quantities of quantum dots.

6.7 Types of quantum dots

1. Core-shell structures.
2. Lateral quantum dots.

6.7.1 Core-Shell structures

Quantum dots having small regions of one material buried in another with a larger band gap were called as core-shell structures.
Example

1. CdSe in the core
2. ZnS in the shell
3. Ormosil

6.7.2 Lateral Quantum Dots

Individual quantum dots were created from two dimensional electron or hole gases present in remotely doped quantum wells or semi conductor hetro structures called as lateral quantum dots.

6.8 Molecular Cluster Method

1. Large quantities of high quality quantum dots were produced by using chemical precursors in the presence of a molecular cluster.
2. Individual molecules of the cluster would act as a seed or nucleation point.
3. High temperature nucleation was not necessary.
4. Highly scalable method.

6.9 Assembly of quantum dots

1. Viral assembly.
2. Electro chemical assembly.

6.9.1 Viral Assembly

Genetically engineered M13 bacteriophage viruses were used to create quantum dot bio composite structures. Genetically engineered viruses could recognize specific semiconductor surfaces through the method of selection by combinational phase display. The crystalline structures of wild type viruses such as Fd, M13 and TMV were adjusted by controlling

1. The solution concentrations.
2. Solution ionic strength.

3. External magnetic field applied to the solutions.

Advantages

Self assembled quantum dots were obtained highly oriented and self supporting films were obtained from a phase and ZnS precursor solution. Genetic modification and selection were used to vary the length of bacteriophase and the type of inorganic material.

6.9.2 Electrochemical Assembly

Highly ordered arrays of quantum dots were obtained by electrochemical techniques.

6.10 Confinement Potential

Confinement in quantum dots could arise from electrostatic potential generated by

1. External electrodes.
2. Doping.
3. Strain.
4. Impurities.

The energy spectrum of the quantum was controlled by

1. Size.
2. Shape and
3. Strength of the confinement potential.

6.11 Investigation

Tunnelling spectroscopy was used for the investigation of quantum dots.

6.12 Artificial Atoms

The discrete transitions in the atomic spectra have resulted in the quantum dots called as artificial atoms.

7. NANO WIRES

Nano structures can be defined as structures that have a thickness or diameter constrained to tens of nano meters or less and an unconstrained length.
At this scale, quantum mechanical effects were important and hence they were called as quantum wires.
Types of nano wires:

1. Metallic nano wire
   Eg: Ni, pt, Au.
2. Semi conducting nano wire
   Eg: Si, InP, GaN.
3. Insulating Nano wire
   Eg : SiO2, TiO2.

Molecular nano wires were of two types:

1. Organic nano wires
   eg: DNA
2. Inorganic nano wires
   Eg: Mo6 S9 Ix.

7.1 Properties

1. It has aspect ratio of 1000. Aspect ratio = length/width.
2. They were called as one dimensional material.
3. Nano wires have interesting properties that were not seen in bulk or 3-D materials.
4. Electrons in nano wires were quantum confined laterally.
5. They occupy energy levels that were different from the traditional continuum of energy levels or bands found in bulk materials.

7.2 Applications

Nano wires were used to link tiny components into extremely small circuits.

8. CONCLUSIONS

In this paper, the basic terms and definitions of nano particles was discussed. The characteristics, advantages and disadvantages of nano technology were also discussed. Applications of nano particles were also mentioned. This paper would be useful to young engineers to study the fundamentals of nano technology. Quantum dots and nano wires were reviewed clearly.

9. REFERENCES

[1] Selvaraj, D. Edison, et al. "Analysis of Efficiency, Thermal Withstanding Capacity and Electromagnetic Interference of Three Phase Squirrel Cage Induction Motor Coated with SiO2 & TiO2 nano composite Filled Enamel." International Journal of Science and Engineering Applications 1.1 (2012): 17- 21.

[2] Edison Selvaraj, D., C. Pugazhendhi Sugumaran, and A. Sivaprakash."Characterization of Electrical and Thermal Properties of Enamel Filled with Carbon Nanotubes." Proceedings of the Third International Conference on Trends in Information, Telecommunication and Computing. Springer New York, 2013.

[3] Selvaraj, D. Edison. "Partial discharge characteristics of enamel filled with micro and nano composite of siO2 and TiO2." International Journal of Science and Engineering Applications 1.2 (2012): 95-101.

[4] Selvaraj, D. Edison. "Characterization of dielectric properties of the enamel filled with carbon nano tubes for the frequency range of 50 Hz-5 MHz" International Journal of Science and Engineering Applications 1.2 (2012): 102-106.

[5] Selvaraj, D. Edison, and C. Pugazhendhi Sugumaran. "Comparative Analysis of Dielectric Properties of Enamel Filled with Various Nanofillers such as ZrO2, Al2O3, CNT and ZnO." International Journal of Science and Engineering Applications 1.1 (2012): 51-55.

[6] Babu, B. Gurukarthik, D. Edison Selvaraj, R. Srinivas, B. Guru Prakash, and R. Vishnu. "Analysis of Relative Permittivity and Tan Delta Characteristics of Silicone Rubber Based Nano-composites." International Journal of Scientific Engineering and Technology , pp.2201-206, 2012.

[7] D. Edison Selvaraj, J. Ganesan. "Experimental Analysis of Efficiency and Thermal Withstanding Capacity of Three Phase Squirrel Cage Induction Motor Coated with SiO2 & TiO2 Nano Composite Filled Enamel", International Journal of Engineering Sciences, Vol (2), No (4), 2013. pp. 115-118.

[8] Lieutenant Ganesan. J, Jeyadevi.S.Dr, and Edison Selvaraj. D, "Performance Analysis of Single Phase Induction Motor Coated with Al2O3 Nano Filler Mixed Enamel" ACEEE International Journal on Recent Trends in Engineering & Technology Vol. 10, No. 1, Jan 2014.

[9] Edison Selvaraj. D, Pugazhendhi Sugumaran. C, Lieutenant Ganesan. J, Ramathilagam. J, "Analysis of Dielectric and Thermal Properties of Polyamide Enamel Filled with Carbon Nano tubes" International Journal of Nano science, Vol.12, Issue 3, June 2013.

[10] Lieutenant Ganesan. J, Edison Selvaraj. D, and Ramathilagam. J,"Experimental analysis of Thermal conductivity of enamel filled with micro and nano composite of SiO2 and TiO2" International journal of Advanced Research in Electrical, Electronics and Instrumentation Engineering, Vol.2, Issue 7,pp. 2907-2912 , 2013.

[11] Lieutenant Ganesan. J, Jeyadevi. S. Dr, and Edison Selvaraj. D, "Reduction of Electromagnetic Interference in Single Phase Induction Motor by coating the winding with Al2O3 nano filler mixed Enamel" International journal of Advanced Research in Electrical, Electronics and Instrumentation Engineering, Vol.2, Issue7,pp. 2913-2916 , 2013.

[12] Lieutenant Ganesan. J, Edison Selvaraj. D, and Selva Kumar. B, "High Efficiency Induction Motor", International journal of Advanced Research in Electrical, Electronics and Instrumentation Engineering, Vol.2, Issue 2, pp. 750-754, 2013.

[13] Lieutenant Ganesan. J, Edison Selvaraj. D, GuruPrakash. B, Vishnu Prakash. R, Muthupandi. E, and BalaKumar. R, "Analysis of Efficiency and Thermal Withstanding Capacity of Single Phase Induction Motor Coated with Al2O3 Nano Filler Mixed Enamel", International journal of Advanced Research in Electrical, Electronics and Instrumentation Engineering, Vol.2,Issue 3,pp. 960-963, 2013.

International Journal of Science and Engineering Applications
Volume 3 Issue 5, 2014, ISSN-2319-7560 (Online)

Effect of Rotor Angle Displacement on Synchronous Generator Transient Condition under Three-phase Fault

Thu Zar Mon
Department of Electrical Power Engineering,
Mandalay Technological University,
Mandalay, Myanmar

Yan Aung Oo
Department of Electrical Power Engineering,
Mandalay Technological University,
Mandalay, Myanmar

Abstract: This paper approaches the effect of change of rotor angle upon armature current due to short circuit condition at the terminal of the synchronous generator. The synchronous machine as an AC generator, driven by the turbine to convert mechanical energy to electrical energy, is the major electric power-generating source throughout the world. The severest condition of three-phase short-circuit waveform is naturally higher than the steady-state condition concerning with AC component of armature current, because armature reactances change due to armature reaction. The Park's equations are solved numerically during balanced three-phase short-circuit. Under three-phase fault is applied at the terminal of the synchronous generator, the fault current waveforms of i_a, i_b, i_c and i_F are observed for the various rotor angle displacements, i.e, δ=0°, δ=30°, δ=60° and δ=90°. The transformed quantities are obtained from the projection of the actual variable on three axis; one along the direct axis, a second along the quadrature axis, and the third on a stationary axis. The interest is to study the wave form of the currents of the armature and field windings under three-phase short-circuit at the terminal of synchronous machine by using the MATLAB program.

Keywords: Park transformation, rotor angle, symmetrical fault, synchronous machine, transient

1. INTRODUCTION

In large interconnected power system, the synchronous machine includes as a main part in the application and operation of electric supply. The synchronous machine as an ac generator, driven by the turbine to convert mechanical energy to electrical energy, is the major electric power-generating source throughout the world [1].In this paper, the resulting differential equations describing the synchronous machine's characteristic due to the short circuit condition of three phase fault. These nonlinear equations are transformed into linear differential equations using Park's transformation. MATLAB is used with ease to simulate the nonlinear differential equations [2]. The events within a generator subjected to a sudden short-circuit depend on several factors; including (i) the instant in the cycle at which short-circuit is initiated (ii) the load and excitation of the machine at this time.

2. PROBLEM STATEMENT

Under transient conditions, such as short circuits at generator terminal, the flux linkages with the rotor circuits change with time. This result of transient currents in all rotor circuits reacts on armature [3].For the transient analysis, the idealized synchronous machine is represented as a group of magnetically coupled circuits with inductances, which depend on angular position of the rotor. The resulting differential equations describing the machine have time varying coefficients, and a closed form of solution in most cases is not feasible.

3. SYNCHRONOUS MACHINE TRASIENT

The synchronous machine consists of three stator windings mounted on the stator, and one field winding mounted on the rotor. Two additional fictitious windings could be added to the rotor, one along the direct axis and one along the quadrature axis, which model the short-circuited paths of the damper windings. These windings are shown schematically in Figure 1.

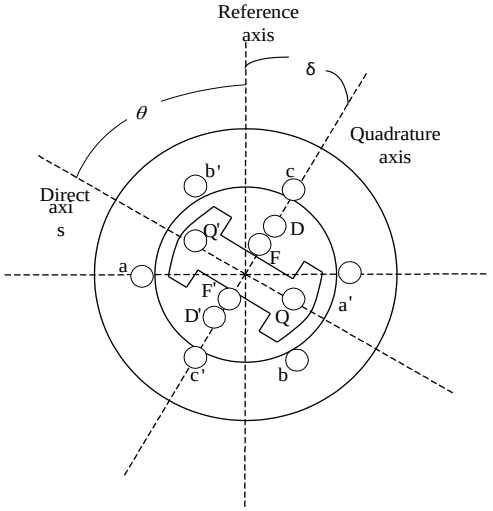

Figure 1. Schematic representation of a synchronous machine

Assuming a synchronously rotating reference frame (axis) is rotating with the synchronous speed ω which will be along the axis of phase a at $t = 0$. If θ is the angle by which rotor direct axis is ahead of the magnetic axis of phase a, then

$$\theta = \omega t + \delta + \pi/2 \quad (1)$$

Where, δ is the displacement of the quadrature axis from the synchronously rotating reference axis and $(\delta + \pi/2)$ is the displacement of the direct axis.

In the classical method, the idealized synchronous machine is represented as a group of magnetically coupled circuits with inductances, which depend on the angular position of the rotor. In addition, saturation is neglected and spatial distribution of armature mmf is assumed sinusoidal [4].

4. PARK TRANSFORMATION

Park Transformation is a well-known technique in the analysis of electric machines, where the three rotating phases abc are transferred to three equivalent stationary dq0 phases (d-q

reference frame). A great simplification can be made by transformation of stator variables from phases *a*, *b*, and *c* into new variables the frame of reference of which moves with the rotor. The transformation is based on the so-called two-axis theory [5].

The transformed quantities are obtained from the projection of the actual variables on three axes; one along the direct axis of the rotor field winding, called the direct axis; a second along the neutral axis of the field winding, called the quadrature axis; and the third on a stationary axis. The three armature currents i_a, i_b, and i_c are replaced by three fictitious currents with the symbols i_d, i_q, and i_0. They are found such that, in a balanced condition, when $i_a + i_b + i_c = 0$, they produce the same flux, at any instant, as the actual phase currents in the armature. The third fictitious current i_0 is needed to make the transformation possible when the sum of the three-phase current is not zero [6].

The Park transformation for currents is as follows

$$\begin{bmatrix} i_0 \\ i_d \\ i_q \end{bmatrix} = \sqrt{2/3} \begin{bmatrix} 1/\sqrt{2} & 1/\sqrt{2} & 1/\sqrt{2} \\ \cos\theta & \cos(\theta - 2\pi/3) & \cos(\theta + 2\pi/3) \\ \sin\theta & \sin(\theta - 2\pi/3) & \sin(\theta + 2\pi/3) \end{bmatrix} \begin{bmatrix} i_a \\ i_b \\ i_c \end{bmatrix} \quad (2)$$

or, in matrix notation

$$i_{0dq} = \mathrm{P} i_{abc} \quad (3)$$

Similarly for voltages and flux linkages,

$$v_{0dq} = \mathrm{P} v_{abc} \quad (4)$$

$$\lambda_{0DQ} = \mathrm{P} \lambda_{ABC} \quad (5)$$

P matrix is augmented with a 3 x 3 identity matrix U (unit matrix) to get;

$$\begin{bmatrix} \lambda_{0dq} \\ \lambda_{FDQ} \end{bmatrix} = \begin{bmatrix} P & 0 \\ 0 & U \end{bmatrix} \begin{bmatrix} \lambda_{abc} \\ \lambda_{FDQ} \end{bmatrix} \quad (6)$$

$$\text{or} \quad \begin{bmatrix} \lambda_{abc} \\ \lambda_{FDQ} \end{bmatrix} = \begin{bmatrix} P^{-1} & 0 \\ 0 & U \end{bmatrix} \begin{bmatrix} \lambda_{0dq} \\ \lambda_{FDQ} \end{bmatrix} \quad (7)$$

Transforming the stator-based currents (i_{abc}) into rotor-based currents (i_{0dq}), with rotor currents unaffected,

$$\begin{bmatrix} i_{abc} \\ i_{FDQ} \end{bmatrix} = \begin{bmatrix} P^{-1} & 0 \\ 0 & U \end{bmatrix} \begin{bmatrix} i_{0dq} \\ i_{FDQ} \end{bmatrix} \quad (8)$$

$$\text{or} \quad \begin{bmatrix} i_{abc} \\ i_{FDQ} \end{bmatrix} = \begin{bmatrix} P^{-1} & 0 \\ 0 & U \end{bmatrix} \begin{bmatrix} i_{0dq} \\ i_{FDQ} \end{bmatrix} \quad (9)$$

Once a solution is obtained for the direct axis and quadrature axis currents, the phase currents are obtained through the inverse Park transformation.

$$i_{abc} = \mathrm{P}^{-1} i_{0dq} \quad (10)$$

Substituting for P^{-1} from (4), and noting $i_0 = 0$, the phase currents are

$$\begin{aligned} i_a &= i_d \cos\theta + i_q \sin\theta \\ i_b &= i_d \cos(\theta - 2\pi/3) + i_q \sin(\theta - 2\pi/3) \\ i_c &= i_d \cos(\theta + 2\pi/3) + i_q \sin(\theta + 2\pi/3) \end{aligned} \quad (11)$$

5. PROGRAM APPLICATION PACKAGE

The flow chart for three-symmetrical short-circuits and "symshort" function diagrams are as shown in Figure 2 and Figure 3.

The software package is an environment for power system analysis running under the Microsoft Windows platform operating system MATLAB is the programming language contributing to the current development of the software package. The software environment is conceptually structured in the form of a tree.

The purpose of this tree structure is to facilitate the future extension of the package and accessibility of all the modules of the environment and at the same time assist the user in choosing the correct next module.

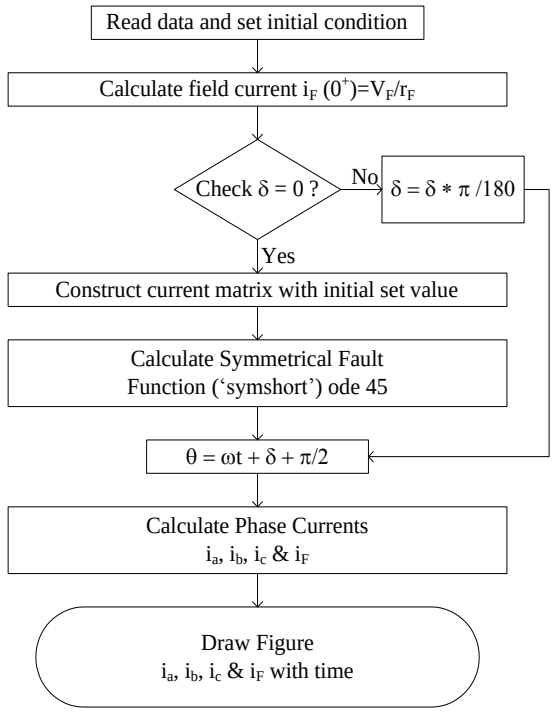

Figure 2. Flow Diagram for Symmetrical Three-Phase Short-Circuit

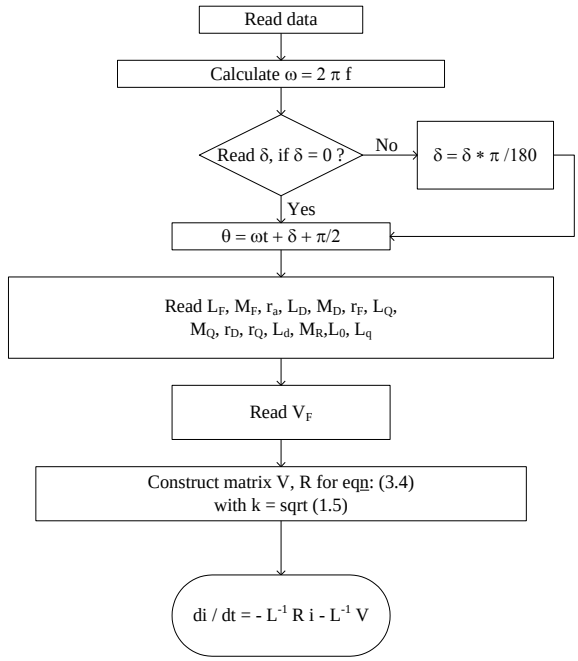

Figure 3. Flow Diagram of function "symshort" for Symmetrical Three-Phase Short-Circuit

6. BALANCED THREE-PHASE SHORT CIRCUIT WAVEFORM

If θ is the angle by which rotor direct axis is ahead of the magnetic axis of phase a, then

$\theta = \omega t + \delta + \pi/2$ (shown in equation 1)
By changing δ as 0°, 30°, 60° and 90°, the angle θ will be changed. Changing of angle θ will affect on phase current i_a, i_b and i_c as shown in equation (11).
In three phase symmetrical system, the phase angle between i_a, i_b and i_c are 120° apart each other. If we let i_a in x-axis at positive side, i_b will be 60° leading and i_c will be 60° lagging. The simulation results are as shown in Figure 4, Figure 5, Figure 6 and Figure 7 if we changed δ=0°, 30°, 60° and 90° alternatively. According to the simulation results, the results of Figure 4(a), Figure 4(b) and Figure 7(c) are the same in magnitude and different in phase angle. Next, the result of Figure 4(c), Figure 7(a) and Figure 7(b) are the same in magnitude and different in phase angle. Then, the results of Figure 5(a), Figure 5(b) and Figure 6(c) are the same in magnitude and different in phase angle. Finally, the results of Figure 5(c), Figure 6(a) and Figure 6(b) are the same in magnitude and different in phase angle. The simulation results of i_F is the same in all Figure 4(d), Figure 5(d), Figure 6(d) and Figure 7(d).
Neglecting of all winding resistances will result in considerable numerical simplification, at a very convenient in lost accuracy.

$$i_a(0^+) = i_b(0^+) = i_c(0^+) = 0 \tag{12}$$

$$i_0(0^+) = i_d(0^+) = i_q(0^+) = 0 \tag{13}$$

The initial value of the field current is

$$i_F(0^+) = \frac{V_F}{r_F} \tag{14}$$

For balanced three-phase short circuit at the terminals of the machine

$$v_a = v_b = v_c = 0 \tag{15}$$

Since $i_0 = 0$, the machine equation in the rotor reference frame following a three-phase short circuit becomes

$$\begin{bmatrix} v_d \\ -v_F \\ 0 \\ v_q \\ 0 \end{bmatrix} = -\begin{bmatrix} r & 0 & 0 & \omega L_q & \omega kM_Q \\ 0 & r_F & 0 & 0 & 0 \\ 0 & 0 & r_D & 0 & 0 \\ -\omega L_d & -\omega kM_F & -\omega kM_D & r & 0 \\ 0 & 0 & 0 & 0 & r_Q \end{bmatrix} \begin{bmatrix} i_d \\ i_F \\ i_D \\ i_q \\ i_Q \end{bmatrix} - \begin{bmatrix} L_d & kM_F & kM_D & 0 & 0 \\ kM_F & L_F & M_R & 0 & 0 \\ kM_D & M_R & L_D & 0 & 0 \\ 0 & 0 & 0 & L_q & kM_Q \\ 0 & 0 & 0 & kM_Q & L_Q \end{bmatrix} \frac{d}{dt} \begin{bmatrix} i_d \\ i_F \\ i_D \\ i_q \\ i_Q \end{bmatrix} \tag{16}$$

This equation is in the state-space form and can be written in compact form as

$$v = -Ri - L\frac{d}{dt}i \tag{17}$$

$$\frac{d}{dt}i = -L^{-1}Ri - L^{-1}v \tag{18}$$

6.1 Synchronous Machine Parameters

A three-phase model, which uses direct physical parameters, is well suited for simulation on a computer. And it is not necessary to go through complex transformations. The analysis can easily be extended to take the speed variation into account by including the dynamic equations of the machine. In this paper, assuming the machine data are as follow:
A 500-MVA, 30-kV, 50-Hz synchronous generator is operating at no-load with a constant excitation voltage of 400V.

The generator parameters for all Problems are

L_d = 0.0072 H L_q = 0.0070 H L_F = 2.500 H

L_D = 0.0068 H L_Q = 0.0016 H M_F = 0.100 H

M_D = 0.0054 H M_Q = 0.0026 H M_R = 0.125 H

r = 0.0020 Ω r_F = 0.4000 Ω r_D = 0.015 Ω

r_Q = 0.0150 Ω L_0 = 0.0010 H

A three-phase short circuit occurs at the armature terminals. Use ode45 to simulate equation (16), and obtain the transient waveforms for the current in each phase and the field current.

6.1.1 Case Study 1

Assume the short circuit is applied at the instant when the rotor direct axis is along the magnetic axis of phase a, i.e.,δ=0. Also, assume that the rotor speed remains constant at the synchronous value.
The dc field voltage is V_F = 400 V. The derivatives of the state equation given by equation (18), together with the coefficient matrices in equation (16) are defined in a function file named symshort.m, which returns the state derivatives. The initial value of the field current is

$$i_F(0^+) = \frac{V_F}{r_F} = \frac{400}{0.4} = 1000 \text{ A}$$

and since the machine is initially on no-load.

$$i_0(0^+) = i_d(0^+) = i_q(0^0) = 0$$

The program file cs2.m from appendix uses ode45 to simulate the differential equations defined in symshort over the desired interval. The periodic nature of currents necessitates a very small step size for integration. The currents i_d and i_q are substituted in equation (11) and the phase currents are determined. The results of the simulations of i_a, i_b, i_c and i_F are shown in Figure 4.

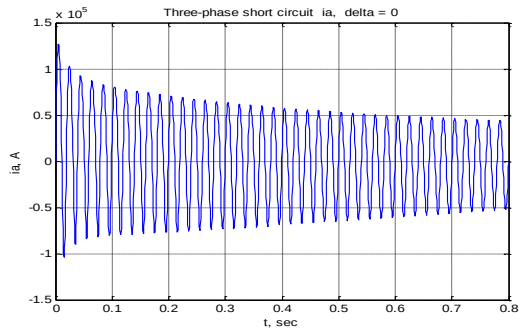

(a)

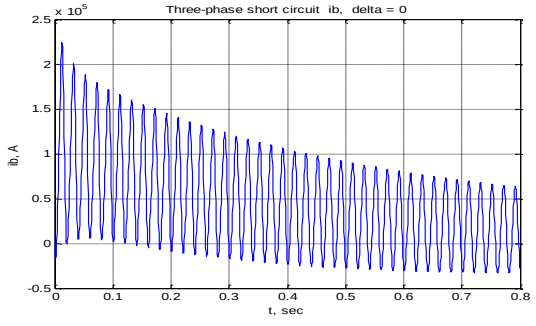

(b)

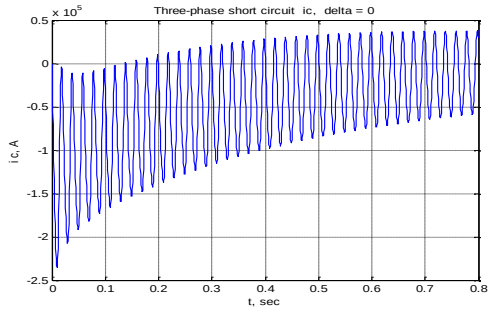

(c)

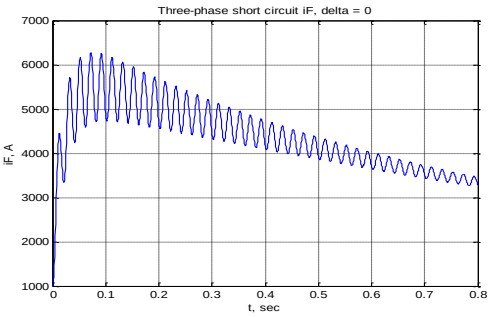

(d)

Figure 4. Balanced three-phase short-circuit current waveforms

6.1.2. Case Study 2

If the machine angle, δ, is increased from 0° to 30°, the waveforms of i_a, i_b, i_c and i_F are shown in Figure 5.

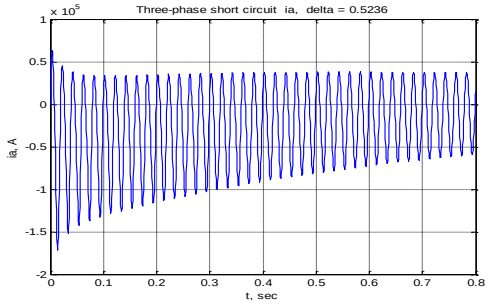

(a)

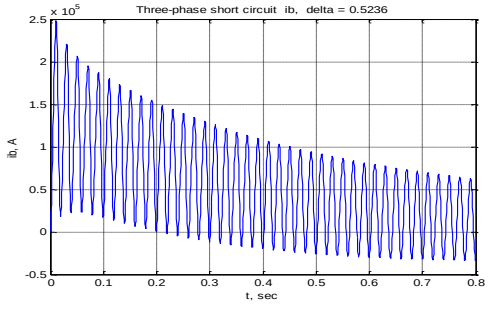

(b)

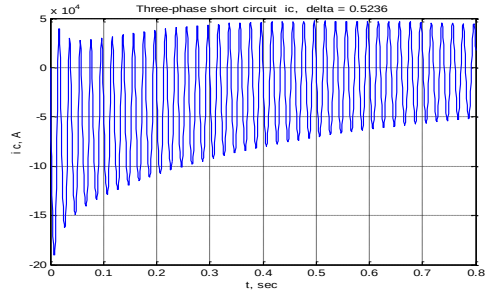

(c)

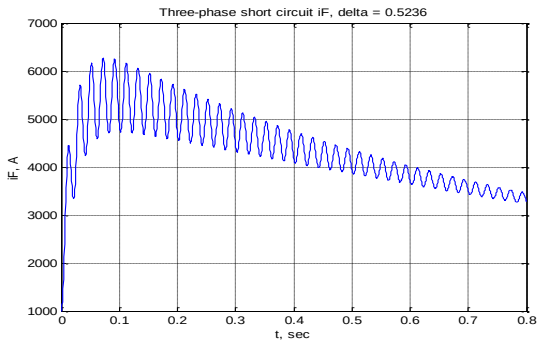

(d)

Figure 5. Balanced three-phase short-circuit current waveform at machine terminal (30°)

This case study shows that rise of rotor angle is found to shift waveform position of armature currents. The settling time changes in small amount and i_F is found to be unchanged.

6.1.3. Case Study 3

If the machine angle, δ, is increased from 0° to 60° the waveforms of i_a, i_b, i_c and i_F are shown in Figure 6.

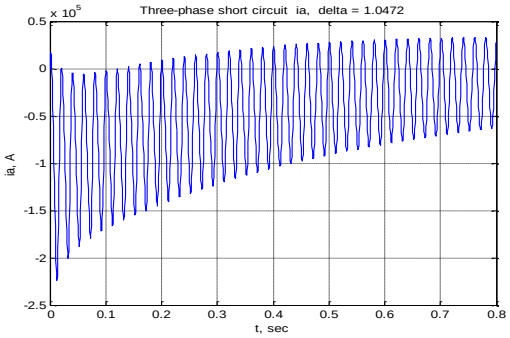

(a)

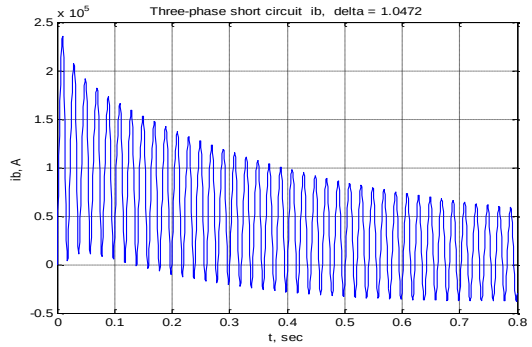

(b)

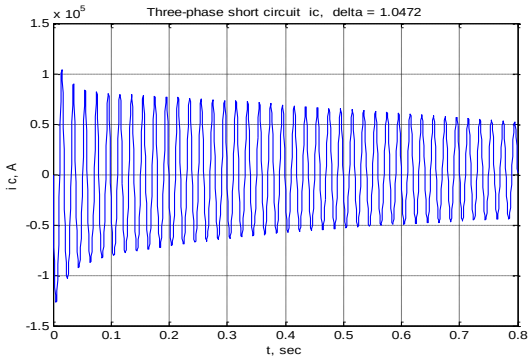

(c)

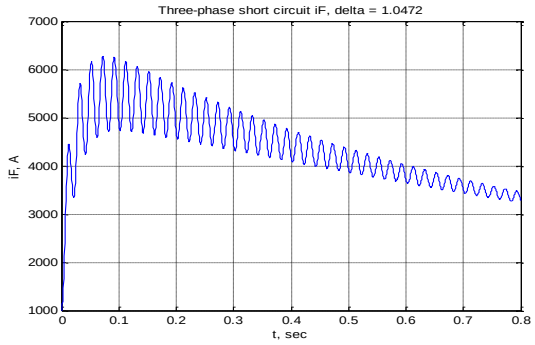

(d)

Figure 6. Balanced three-phase short-circuit current waveform at machine terminal (60°)

6.1.4. Case Study 4

If the machine angle, δ, is increased from 0° to 90° the waveforms of i_a, i_b, i_c and i_F are shown in Figure7.

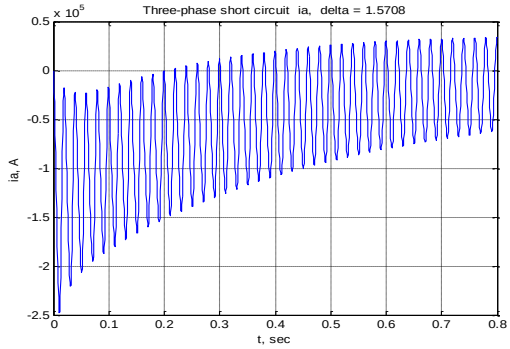

(a)

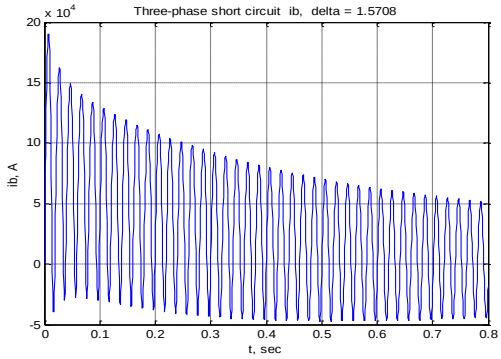

(b)

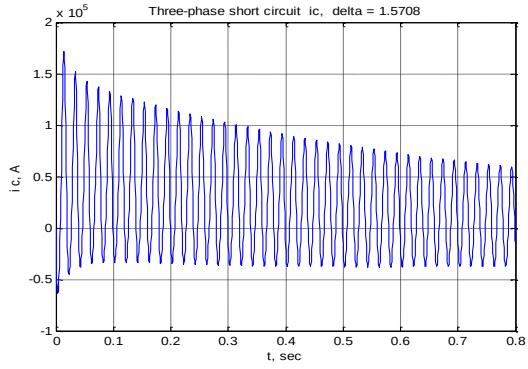

(c)

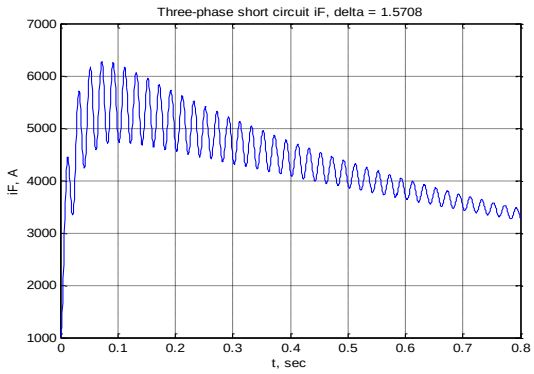

(d)

Figure 7. Balanced three-phase short-circuit current waveform at machine terminal (90°)

The stated testings are found to give the design criteria and three-phase short circuit condition of a synchronous generator.

7. CONCLUSION

This paper has analyzed the conditions of three-phase short circuit on the terminals of the synchronous generator. A sudden three-phase short circuit is applied to the terminals of an unloaded generator and the waveform of the current is obtained by using the MATLAB program. Synchronous machines naturally operate at constant speed. But at transient condition, speed varies and thus the rotor angle δ changes causing instability. According to the simulation results, it can be seen that the fault current magnitude of phase a, b and c are remain the same while the rotor angle displacement varies. But the phase shift (or) the DC offset is occurred respectively with respect to the different rotor angles. Moreover, it can also be seen that the magnitude of field winding current at transient condition is significant but they are independent of rotor angle displacement. Furthermore, if the field voltage is increased, the magnitude of the fault current levels of i_a, i_b, i_c and i_F increase and when the field voltage is decreased, the magnitude of the fault current levels of i_a, i_b, i_c and i_F also decrease.

8. ACKNOWLEDGMENT

The author would like to express her gratitude to Dr. Khin Thuzar Soe, Associate Professor and Head of Electrical Power Engineering Department, Mandalay Technological University and Dr.Yan Aung Oo, Associate Professor, Department of Electrical Power Engineering, Mandalay Technological University for his encouragement and helpful suggestion and supervision. The author wishes to thanks all teachers. Thanks are also extended to her dear parent and friends for their support.

9. REFERENCES

[1] Adkins, General Theory of Electrical Machines, Chapman & Hall, 1975

[2] Biran, A., and Breiner, M. 1996. MALAB for Engineer

[3] Hubert, C.I. 1991.Electric Machines

[4] I. R. Smith and S. Sriharan, Transient Performance of Induction Machines. Proc. IEE, 133, 1173, 1966.

[5] Kundur, P.1994. Power System Stability and Control

[6] M. G. Say, Alternating Current Machine, Pitman Publishing Ltd, 4th Edition, 1976.

[7] P. J. Lawrence and J. M. Stevenson, Induction Machine Performance with a Variable Frequency Supply, Proc. IEE, 113, 1617, 1966.

[8] Saadat, H. 1999. Power System Analysis Singapore: McGraw-Hill Co.

[9] Elgerd, O.I. 1971. Electric Energy System Theory: An Introduction U.S.A.: McGraw-Hill Book Co.

International Journal of Science and Engineering Applications
Volume 3 Issue 5, 2014, ISSN-2319-7560 (Online)

Different Approach of VIDEO Compression Technique: A Study

S. S. Razali
Faculty of Electronic and Computer Engineering
Universiti Teknikal Malaysia Melaka (UTeM)

N. M. Z. Hashim
Faculty of Electronic and Computer Engineering
Universiti Teknikal Malaysia Melaka (UTeM)

S. Z. Yahya
Faculty of Electronic and Computer Engineering
Universiti Teknikal Malaysia Melaka (UTeM)

K. A. A. Aziz
Faculty of Engineering Technology
Universiti Teknikal Malaysia Melaka (UTeM)

A.Salleh
Faculty of Electronic and Computer Engineering
Universiti Teknikal Malaysia Melaka (UTeM)

N. R. Mohamad
Faculty of Electronic and Computer Engineering
Universiti Teknikal Malaysia Melaka (UTeM)

Abstract: The main objective of video compression is to achieve video compression with less possible losses to reduce the transmission bandwidth and storage memory. This paper discusses different approach of video compression for better transmission of video frames for multimedia application. Video compression methods such as frame difference approach, PCA based method, accordion function, fuzzy concept, and EZW and FSBM were analyzed in this paper. Those methods were compared for performance, speed and accuracy and which method produces better visual quality.

Keywords: Compression, Losses, Memory, Transmission Bandwidth, Video Compression.

1. INTRODUCTION

Moving video images also call video is a main component in internet world today. Video are integrated into the application, website and almost everything that demand the need for moving video images. The need for fast, reliable and high quality video has taken the video compression technology into the next level [1]-[5]. Video compression is a technique that was used reduces redundancy and also reduces the number of bits needed to send or store the video. This paper summarize difference technique or method used in video compression, these method are [6] accordion function, [7] EZW and FMBW, [8] fuzzy concepts, [9] frame difference approach and lastly [10] PCA method.

2. METHODS OF VIDEO COMPRESSION

2.1 Method 1: Accordion Function

This paper will focus on reducing the storage space for video signal [6]. Figure 1 shows process for block diagram of video compression.

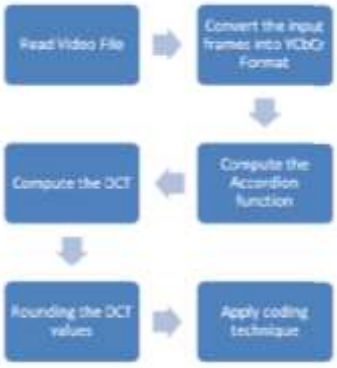

Figure 1: Block diagram of video compression

The technique compressed that involved in this process is removal of spectral redundancy and removal of temporal redundancy. Reduce redundancy which reduce number of bits in order to transmit or keep video data is known as video compression.

2.1.1 Video compression process

2.1.1.1 Removal of spectral redundancy

Basic color consists of RED, GREEN and BLUE color, it represent 8 bit of each color which it 24 bits in total to represent any color by adding different proportion of basic color together. This means need more bits to show color information of the given frame and also known as spectral redundancy. The RED, GREEN and BLUE (RGB) need to convert into YCbCr format in order to reduce number of bits. Y introduced as Luminance component of the image, Cb as chrome for blue color and Cr as chrome for red color. Luminance or Luma represent variation between white to black shades and for chrome it represents color information. By using equation (1) and (3) respectively below the color format of different type of video frames can convert into YCbCr format:

$$Y = 0.299R + 0.587 + 0.114 \dots (1)$$

For PAL:

$$U = 0.493\ (B - Y) \dots (2)$$

$$V = 0.877(R - Y) \dots (3)$$

PAL stands for Phase Alteration in Line. Figure 2 to Figure 3 is result image when the frame is converted into

YCbCr format. Figure 3 present the luminance values, Figure 4 present the Cb values and Figure 5 present the Cr values for the input frame. From the beginning input video, different frames were taken and assign those into structure and finally were converted into YCbCr format.

Figure 2: Video Frame

Figure 3: Luminance component

Figure 4: Cb component

Figure 5: Cr component

Computation of accordion function is presented by four consecutive video frames above as result. These four steps were repeated in Figure 10 for all input video frames.

2.1.1.2 Removal of temporal of redundancy

Temporal redundancy is frequently present between a set of frames which it takes only a few portion of each frame itself involved with any motion that take part.

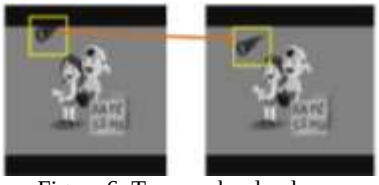

Figure 6: Temporal redundancy

Refer to Figure 6, the yellow box contains motion and all other areas were constant called temporal redundancy. Accordion is a process converted redundancy into spatial redundancy. Temporal redundancy known as non-changing data amount, by placing the successive frames adjacent to each other it can eliminate the constant data in successive frames. It can achieve by using accordion present of 4 successive frames.

Four consecutive groups of frames were taken and merge to create an image in Accordion. The input video of size M times N times 500 bits. Figure 7 shows its accordion representation.

The corresponding column pixels were places adjacent to each consecutive frame's column. Refer to input video the consecutive frames from 104 to 108 frame numbers are present in Figure 8 (a), Figure 8 (b), Figure 9 (c) and Figure 9 (d) respectively. Using shift and merge operations, the accordion function was computed on these frames, which represents the temporal redundancy as spatial representation (Figure 10).

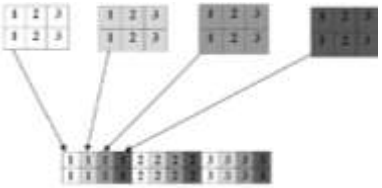

Figure 7 Accordion

Figure 8 (a) to (b)

Figure 9 (a) to (b)

Figure 10

2.2 Method 2: EZW and FSBM

Method that been used in this paper is EZW and 7 different algorithms type of block matching algorithms that use in video compression for motion estimation [7]. 7 different algorithms: Exhaustive Search (ES), Three Step Search (TSS), New Three Step Search (NTSS), Simple and Efficient Search (SES), Four Step Search (4SS), Diamond Search (DS) and Adaptive Rood Pattern Search (ARPS).

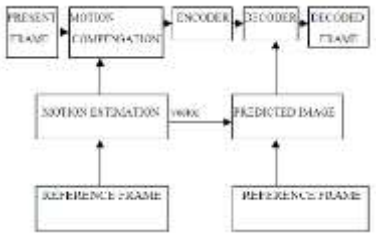

Figure 11: Block diagram for video compression process flow

EZW stands for embedded zero tree wavelet algorithm, it simple and effective image compression and make the bits in the bit stream generate in terms of importance yet yielding a complete embedded code. A sequence of binary decisions that remove an image from the null image is representing the embedded code. By using it, at any point encoder locate the encoder can dismiss it, this allow a target rate to be met exactly. Furthermore, EZW consistency produces a compression result to produce a fully embedded bit stream. In order to achieve with this technique it requires no codebooks or training or knowledge of the image store.

2.2.1 Block Matching Algorithms

Every pixel within a macro block produce one motion vector for each macro block has some motion activity. The main idea is to divide the current frame into number of macro blocks of fixed size. Also to create a motion vector which it will comprises the location of the macro block of the current frame in the previous frame. As always the macro block is approach as a sequence of sixteen pixels and the search area is seven pixels on all 4 sides in pervious frame of the corresponding macro block. Based on the output of cost functions it can create the matching of one macro block with other.

7 different algorithms type of block matching algorithms:

i. Exhaustive search (ES).

Known as Full Search, is the most expansive algorithm of all. This block matching algorithm calculates the cost function location in the search window as result; it gives the highest Peak-Signal-to-Noise-Ratio (PSNR) and finds the best match that it can get. However there is a disadvantage using ES which is the larger search window the more computations need.

ii. Three Step Search (TSS)

The earliest in fast block matching back to middle 1980s. TSS search and picks the one that give less cost and can make it as new search origin.

iii. New Three Step Search (NTSS)

To reduce cost of computational the TSS improved to NTSS, New Three Step Search. NTSS having provisions for half way stop and supply a center biased searching scheme.

iv. Simple and Efficient Search (SES)

SES is another sub to TSS. In opposite direction it cannot be 2 minimum unimodal surfaces and for eight point which its fixed pattern search of TSS can save on computation by changed it to incorporate. The algorithm same as TSS three steps but the innovation make each steps has more 2 phases.

v. Four Step Search (4SS)

Not to different from NTS, 4SS also have center biased searching itself and halfway stop provision. For the first step, pattern size of 4SS is fixed to S = 2 no matter what the *p* parameter value is.

vi. Diamond Search (DS

Block matching algorithm DS is exactly the same as 4SS, but the search point pattern which is square changed into diamond pattern and for algorithm there is no limit on the number of steps make this algorithms can find global minimum accurately. 2 difference types of pattern in DS which are Large Diamond Search Pattern (LDSP) and Small Diamond Search Pattern (SDSP). The 1st steps use LDSP and last steps use SDSP.

vii. Adaptive Rood Pattern Search (ARPS)

ARPS show that the fact of general motion in a frame is coherent. Use the predicted motion vector to check the location pointed and it also can checks at a root distributed points.

Figure 12: Original image

Figure 13: Compressed image using EZW method

Figure 14: Compression image using artificial colors.

As result the original size of the video is 25 Mega Byte and the compression video size is reduced to 21.3 Mega Byte. The compression is complete with a good achievement through compression ratio and factor.

2.3 Method 3: Fuzzy concepts

This paper focused on the fuzzy concept in the video compression sector with H.264 algorithms and MPEG4 [8]. By applying H.264 in medical video compression and then improve the rate control of H.264 algorithm with better quality. In order to implement it, there is three steps to follow:

i. H.264 need to reviewed and meet the area medical video compression.
ii. A new fuzzy based algorithm is introduce to each frame of the video and make compression of based H.264.
iii. Step is make two comparison between H.264 and MPEG-4 and comparison between JVT-H014 (old version of H.264 algorithm) and proposed fizzy concept. Motion Picture Experts Group (MPEG4) and H.263 are standards that are based on video compression.

a) New fuzzy scheme

The frames will be fuzzified and then fuzzy based segmentation is applied to it is created by a new brand algorithm so each of medical images will have more background that usually it only has ROI. Then the isolation begins. In result it shows the minimum will be compression and the maximum is to the background. The cons with the medical video compression are that some artifacts can always induced inside which make the doctors see a false conclusion. For better result use fuzzy method along with optimum bit rate scheme.

b) Comparison between MPEG-4 and H.264

Table 1 represent the results gain from H.264 and MPEG-4 without put any rate control. For each sequence, as the target bit rates which are 4 bit rates from high to low are selected. The difference between H.264 and MPEG-4, refer to PSNR gain and bit rate saving in the table.

Table 1: Result achieved using MPEG-4 and H.264

Sequence	Target Bit Rate (kbps)	PSNR (dB)		PSNR Gain (dB)	Bit Rate (Kbps)		Bit Rate Saving (%)
		MPEG-4	H.264		MPEG-4	H.264	
CT	238.19	36.12	43.07	6.95	490.93	238.19	2.83
	285.03	35.05	40.55	5.50	303.56	285.03	6.10
	197.55	35.10	37.73	2.63	214.89	197.55	8.07
	145.10	35.07	34.91	-0.16	162.38	145.10	10.64
Echocardiography	2266.14	35.79	38.09	2.30	2266.51	2266.14	0.02
	1317.20	32.94	35.15	2.21	1392.83	1317.20	-1.86
	667.08	30.98	32.44	1.46	703.83	667.08	5.22
	308.26	30.41	29.81	-0.60	327.52	308.26	5.88

When apply in the test medical video sequence, by referring Table 1 it prove that H.264 performance much better than MPEG-4. Means that H.264 is more effective than MPEG-4 and it is an effective alternative solution for medical video applications.

2.4 Method 4: Difference frame approach

This paper discussed about the video compression technique that use algorithm based on frame of video [9]. This technique calculates the frame differencing between the consequences frames according to a specific threshold. This technique concentrated on frames difference approaches that are used in compression technique. There are many stages implemented in this system. Figures 15 show the stages used in this system:

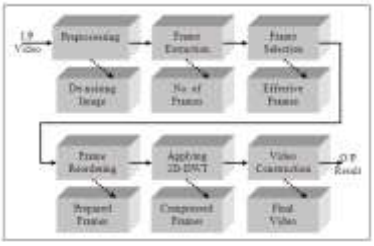

Figure 15: the proposed frame selection key approach

However difference approach is the main core of the system, in which pass the similar frames and select the different frames depends on a certain specified threshold. In addition the selected frames are compressed via applying 2-dimensional discrete wavelet transform.

2.4.1 Frames Difference Approaches for Video Compression

For removing the lowest frame difference, three different methods are used to remove the identical frames in which frames difference approaches among each consecutive frame of extracted frames are applied. The Summary of the structural diagram of the three approaches is shown in Figure 16.

Figure 16: Structural Diagram of frames difference approach

2.4.1.1 Zero Difference Approach

Frames are removed when the gap between any two consecutive frames is zero. This will minimize the number of frames to be re-extracted. Many of the frames difference between consecutive frames are zero; in this case such frames will be removed.

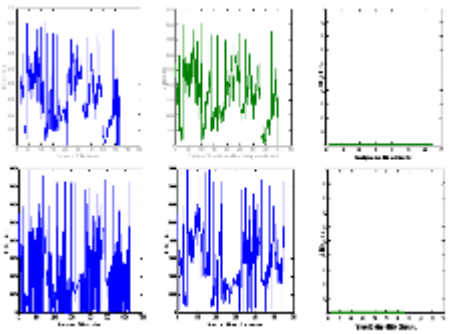

Figure 17: Zero Difference approach

Figures 17, on the left top to bottom represent the frames difference including zero's difference for frames per second 15 and 20 respectively. Middle top to bottom represents frames difference excluding zero's difference frames, while the removed frames in which the frames difference equal to zero are shown in Figures 16 on right top to bottom. As increasing extracting frames per second 10, 15, 20 and 25, the frames difference equal to zero not necessarily increased, since the frames differences in general decreased as the frames per second increased but not exactly equal to zero.

2.4.1.2 Mean Difference Approach

The mean value of the frames difference is calculated. Mathematically the average is acquired by dividing the sum of the observed values of frames difference by the number of observations. Then remove the frames where the frames difference between any consecutive frames is lower than the mean value of the frames difference.

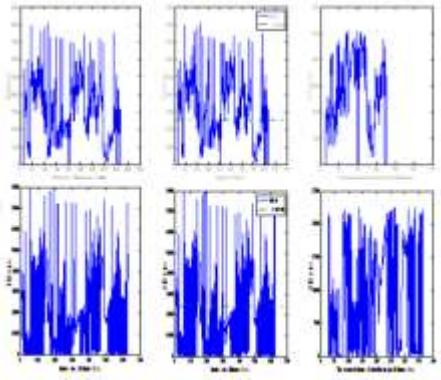

Figure 18: Mean difference approach

Figures 18 from the left top to bottom represent the frames difference including mean's difference for frames per second 15 and 20 respectively. Middle part from top to bottom of the figures represents frames difference including frames below the mean of the overall difference frames; the green line represents the mean of the frames differences. The frames difference above the green line will be maintained and compressed, while the frames difference below the green line will be removed. Left part of the figures represents the frames to be removed. As increasing extracting frames per second, the frames difference decreased and the frames removed are larger

2.4.1.3 Percentage Difference Approach

In this approach different types of videos are examined according to frame details, frame size and the obtained frames differences. This approach concerns mainly in removing the lowest frames difference according to some specific percentage. The percentage depends upon many factors such as compression performance, frame details, frame size and near distance between frames result and analysis.

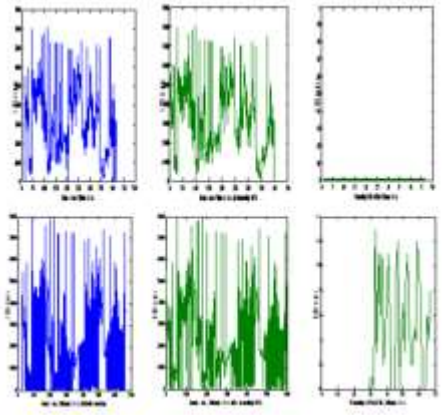

Figure 19: Percentage difference approach

Fi ıt the frames difference for different frames per second 15, & 20 respectively. Middle part from top to bottom of the Figures 4.3 represents frames difference after removing 10% of the lowest frames difference. Left Part of the figures 4.3 represents the frames to be removed. Also different percentages like 15%, 20% were removed of the frames difference.

2.5 Method 5: PCA method

This paper brings up the use of a statistical approach for video compression as new Principle Component Analysis (PCA) based method [10]. Based on necessary of accuracy this method reveals the features of video frames and process them flexibly. This main idea improves the quality of compression effectively. Furthermore this method also focused on the truth that video is a composition of correlated and sequential frames or image, so that the PCA can be applied in and the advantages of using this method is it does not reduce the bandwidth of frequency response, so the progress of frames won't disappear.

2.5.1 PCA method

The values of the components of the matrixes are Mgrayscale N×Pimages. N×Pgrayscale images are equivalent to N×P matrixes. By applying this method, images are move to another part. All images are put in ***X*** matrix that its elements are the intensity values of images.

Considering the first k Eigen vectors from the M Eigen vectors (K<M), the **X** matrix that is a little bit different from **X** matrix. The **X** matrix is compressed matrix which it gain from **X**. So the compression ratio - the ratio of the required memory to save **X** to the neccasary memory to keep **X** - can be determined as below:

$$Memory\ ratio = \frac{requiredmemorytosave\ X}{requiredmemorytosave\ X}$$

2.5.2 IMPROVED PCA

It is available to develop the quality of image exactly and knew the most inaccurate pixels in the reassemble frame or images. The **Y** k matrix is changed to Ŷ k, which to compensate the effect of error the nonzero columns in the bottom of the matrix are applied:

$$\bar{Y}_k = \begin{bmatrix} Y(1,1) & \cdots & Y(1,\alpha) & \cdots & Y(1,N^2-1) & Y(1,N^2) \\ Y(2,1) & \cdots & Y(2,\alpha) & \cdots & Y(2,N^2-1) & Y(2,N^2) \\ \vdots & \vdots & \vdots & \vdots & \vdots & \vdots \\ Y(k,1) & \cdots & Y(k,\alpha) & \cdots & Y(k,N^2-1) & Y(k,N^2) \\ 0 & 0 & Y(k+1,\alpha) & \cdots & 0 & 0 \\ 0 & 0 & Y(k+2,\alpha) & \cdots & 0 & 0 \\ \vdots & \vdots & \vdots & \vdots & 0 & 0 \\ 0 & 0 & Y(M,\alpha) & \cdots & 0 & 0 \end{bmatrix}_{M \times N^2}$$

2.5.3 2DPCA Method

To get image vectors of images construct a high dimensional image vector space the image matrixes need to changed to vectors. This method uses 2D matrixes rather than 1D vectors in conventional PCA and 2DPCA has two fundamental benefit over conventional PCA

a) Easy to design accurate covariance matrixes
b) Because of covariance matrixes size are smaller it took less time to determine corresponding eigenvectors.

2.5.4 Improved PCA and 2DPCA for Video

This part represent the results of applying three mentioned methods above: PCA, Improved PCA and 2DPCA for compression of fourteen sample frames are show. The frames are pick from throwing an apple in a white background. Figure 19 shows the original frames. The frames are organize from the top down and left to right.

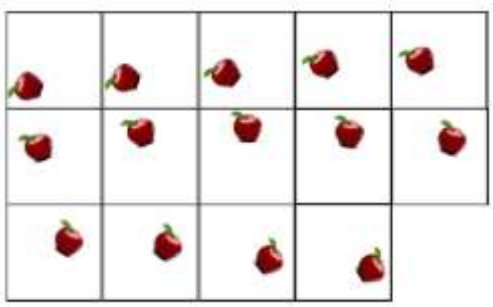

Figure 20 : Based on the background of PCA, 2DPCA and improved PCA in face database compression, the improved PCA shows better results than two other methods.

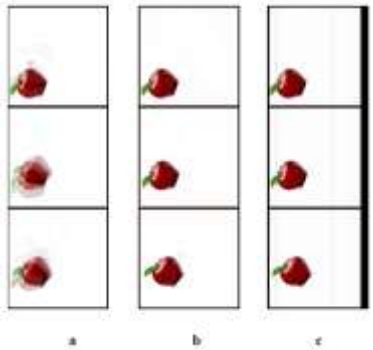

Figure 21: PCA method added fade effects

Figure 21 shows the first three frames of applying mentioned triple methods with same bitrates to the original frames. As it seen, the PCA method added fade effects to the reconstructed frames and applying 2DPCA causes vertical lines and black bands to the frames. So in this application (video compression), the best performance is provided by improved PCA method.

3. DISCUSSIONS

Method	Summary
Accordion function	In this proposed technique, The compressions remove the spectral redundancy and temporal redundancy by using Discrete Cosine Transform and convert into spatial redundancy.
EZW and FSBM	EZW is used as intra compression and seven different block matching algorithm are used for motion estimation in video compression the result are much better if using SPIHT algorithm.
Fuzzy concepts	By using new fuzzy based scheme H.264 video compression are more effective than MPEG-4 for medical video.
Frame different approach	Video compression used algorithm based on frame of video. This technique calculates the frame differencing between the consequences frames or frame near distance according to a specific threshold.
PCA based method	PCA applied to high correlated frame because of video are composition of sequential and correlated frame. The edges of frame do not fade because the PCA method does not reduce the bandwidth of frequency response.

4. CONCLUSIONS

In this paper, five difference methods for video compression are reviewed and discussed. There are still a lot of possibilities for the improvement for lossless, small size, and high quality video for the mentioned method, although these method have a pros and cons. In the end, the best method for video compression are the one that can bring faster, reliable and smaller in size without affecting much on the video quality. All of these requirements is necessary for multimedia application, for user to enjoy the video.

5. ACKNOWLEDGMENTS

We are grateful to Centre for Telecommunication Research and Innovation (CeTRI) and Universiti Teknikal Malaysia Melaka (UTeM) through PJP/2013/FKEKK (29C)/S01215 for their kind and help for supporting financially and supplying the electronic components and giving their laboratory facility to complete this study.

6. REFERENCES

[1] N. M. Z. Hashim, A. F. Jaafar, Z. Zakaria, A. Salleh, and R. A. Hamzah, "Smart Casing for Desktop Personal Computer," International Journal of Engineering and Computer Science (IJECS), vol. 2, no. 8, pp. 2337–2342, 2013.

[2] N. M. Z. Hashim, N. H. Mohamad, Z. Zakaria, H. Bakri, and F. Sakaguchi, "Development of Tomato Inspection and Grading System using Image Processing," International Journal Of Engineering And Computer Science (IJECS), vol. 2 no. 8, pp. 2319-2326, 2013.

[3] N. M. Z. Hashim, N. A. Ali, A. Salleh, A. S. Ja'afar, and N. A. Z. Abidin, "Development of Optimal Photosensors Based Heart Pulse Detector," International Journal Of Engineering and Technology (IJET), vol. 5, no. 4, pp. 3601–3607, 2013.

[4] N. M. Z. Hashim, N. M. T. N. Ibrahim, Z. Zakaria, F. Syahrial, and H. Bakri, "Development New Press Machine using Programmable Logic Controller," International Journal of Engineering and Computer Science (IJECS), vol. 2, no. 8, pp. 2310–2314, 2013.

[5] N. M. Z. Hashim, N. A. Ibrahim, N. M. Saad, F. Sakaguchi, and Z. Zakaria, "Barcode Recognition System," International Journal of Emerging Trends & Technology in Computer Science (IJETTCS), vol. 2, no. 4, pp. 278–283, 2013.

[6] Mitesh Shah, Hetal Patel, *"Design of a New Video Compression Algorithm Using Accordion Function"*, International Journal of Science and Modern Engineering (IJISME) ISSN: 2319-6386, Volume-1, Issue-6, May 2013.

[7] Sangeeta Mishra, Sudhir Savarkar, "*Video Compression Using EZW and FSBM*", International Journal of Scientific and Research Publications, Volume 2, Issue 10, October 2012, ISSN 2250-3153.

[8] MuzhirShaban Al-Ani and Talal Ali Hammouri, *Video Compression Algorithm Based on Frame Difference Approaches* International Journal on Soft Computing (IJSC) Vol.2, No.4, November 2011.

[9] J. Mohanalin Rajarathnam, *A novel Fuzzy based Medical video compression using H.264*, Georgian Electronic ScientificJournal: Computer Science and Telecommunications 2008|No.3 (17).

[10] Mostafa Mofarreh-Bonab, Mohamad Mofarreh-Bonab, *Adaptive Video Compression using PCA Method* International Journal of Computer Applications (0975 – 8887) Volume 44– No.21, April 2012.

International Journal of Science and Engineering Applications
Volume 3 Issue 5, 2014, ISSN-2319-7560 (Online)

Application of Digital Signal Processing In Echo Cancellation: A Survey

D. Jalaputhra
Faculty of Electronic and Computer Engineering
Universiti Teknikal Malaysia Melaka (UTeM)

N. M. Z. Hashim
Faculty of Electronic and Computer Engineering
Universiti Teknikal Malaysia Melaka (UTeM)

M. Izhan Ibrahim
Faculty of Electronic and Computer Engineering
Universiti Teknikal Malaysia Melaka (UTeM)

A.S. Ja'afar
Faculty of Engineering Technology
Universiti Teknikal Malaysia Melaka (UTeM)

A.Salleh
Faculty of Electronic and Computer Engineering
Universiti Teknikal Malaysia Melaka (UTeM)

N. R. Mohamad
Faculty of Electronic and Computer Engineering
Universiti Teknikal Malaysia Melaka (UTeM)

Abstract: The advanced communications world is worried talking more naturally by using hands free this help the human being to talk more confidently without holding any of the devices such as microphones or telephones. Acoustic echo cancellation and noise cancellers are quite interesting nowadays because they are required in many applications such as speakerphones and audio/video conferencing. This paper describes an alternative method of estimating signals corrupted by additive noise or interference. Acoustic echo cancellation problem was discussed out of different noise cancellation techniques by concerning different parameters with their comparative results .The results shown are using some specific algorithms.

Keywords: Acoustic Echo Cancellation (AEC), Adaptive Filtering, Algorithm, Hybrid, Noise Cancellers.

1. INTRODUCTION

The growth of the cellular phone market in the last years has led to an increase on the quality of handset receivers. In particular, the quality of the audio is one of the features the cellular vendors take in high consideration. One issue related to the audio quality is the need for an acoustic echo suppression device which eliminates the far speech signal that propagated between microphones and loudspeaker. Nowadays, the user around the world had used the speaker phones and hands-free phones for their video teleconferencing and audio-conferencing in their daily life and business. It will allow full-duplex communication without having to hold the phone which the data can flow two ways at the same time. Full duplex devices also can communicate back and forth simultaneously.

The existence of echo signal would make conversation difficult. There are several echo signals generated from various factors such as digital network echo and AE (acoustic echo) signal. Most of all, the AE generated between loud-speaker signal and near-end speaker signal, affects the conversation quality significantly, for hands-free set the effective AEC (acoustic echo canceller) is required for better performance. NLMS based the adaptive filtering algorithm is used for AEC because the statistical characteristics of the input signal of the AEC and the echo path are change by time 1. A big reason that is this AEC algorithm for the hands-free fix must operate in real time.

The repetition of sound is called echo which the speech from the far-end caller is transmitted by the speakerphone and transmitted again itself by bouncing off the inside surface. Existence of feedback loop where the far-end caller hears some echo of his own voice is because echoes are picked up by the near-end microphone. One of the effective techniques to reduce this problem is by using the digital signal processing technique as known as acoustic echo cancellation (AEC) or telephone line hybrid echo which it will prevent the feedback and at the same time it will allow full-duplex communication.

Echo can be defined as a waveform which repeated due to reflection from points where the characteristics of the medium through the transmitted wave. It is very useful for the detection and exploration of sonar and radar. In telecommunication system, echo will be influence the quality service. Echo is speech reflection causing the interferences.

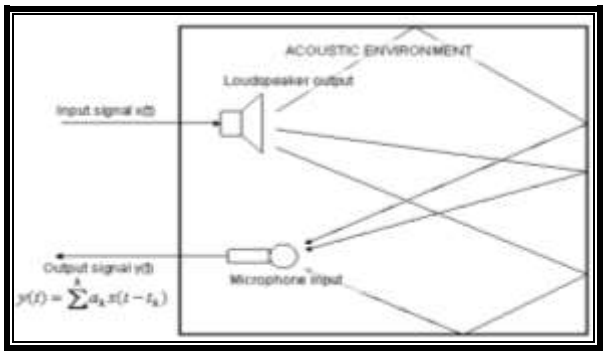

Figure 1: Origin of acoustic echo

In the year 1950's efforts to reduce the echo was carried out by dividing into two types which of acoustic echo and telephone line hybrid echo. As far as possible, it is very important about the echo cancellation because it will increase the quality service in communication service.

2. TYPES OF ECHO

There are two types of echo might be classified with telecommunication which are Acoustic Echo and Line Hybrid Echo.

2.1 Acoustic Echo

A acoustic echo can be explained as sound trap against microphones, then grab sound indicators from your speaker, along with transmits this returning to the originating user. The particular originating user will then hear the particular echo in the user's personal style for the reason that participator echoes.

Acoustic echo is usually become more sensitive as soon as microphones are utilized, and also either the speaker or mike sound system is turned up to as well as if your mike along with speakers is situated so the mike is close to several in the speakers. This specific echo is annoying by simply reflective acoustic echo reflected by simply surfaces and/or physical objects.

Acoustic echo may be caused or made worse while extremely sensitive microphones are utilized, speaker volume is turned up quite high, or the particular microphone along with speaker are extremely close up to each other. So, this may interfere the conversation between participants due to the annoying echo.

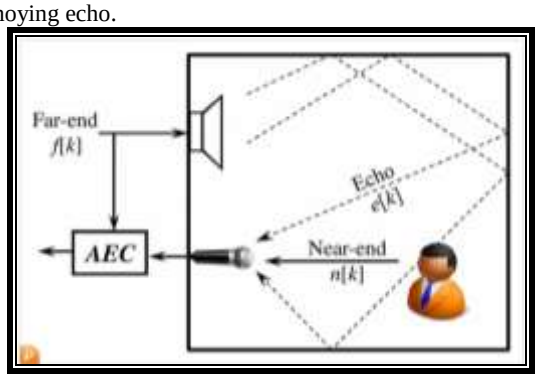

Figure 2: Acoustic Echo

2.2 Hybrid

Hybrid - Essentially the most frequent root cause of indicate in PSTN is impedance1 mismatches in the cross in which 4-wire cell phone circuits are usually transformed into 2-wire circuits. This electrically produced indicate happens if your inward bound vitality in the much end loudspeaker is reflected rear when it comes to your loudspeaker to be a a little bit improved in addition to detained duplication caused by impedance mismatch from the cross. The actual reputation connected with indicate happens each time your replicated signal wait is greater than 10 milliseconds in addition to becomes apparent on the loudspeaker as reflected voice if your wait is greater than as small as sixteen msec. It truly is described on the much end as an improved imitation with the loudspeaker initial.

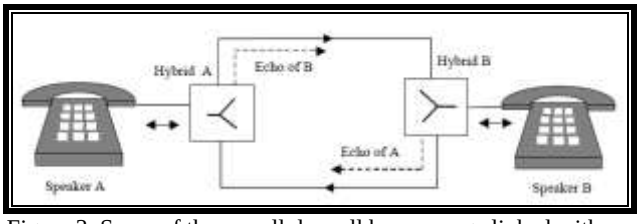

Figure 3: Some of the an cellular call by coverage linked with 2-wire subscriber's using hybrids to 4-wire outlines on the trade

Active hybrid circuits provide a few echo decreases, though not sufficient if the end-to-end circuit delay is even moderate. The network being reflected back is measured as ERL (Echo Return Loss) , the greater the ERL , the lesser the reflected signal back to the speaker . Impedance: the ratio of the electromotive force effective to efficient echo is contrary currents in the electrical circuit for (AC) alternating current to (DC) direct current.

3. ECHO REDUCTION TECHNIQUES

In this section a general survey of echo cancelling technique is presented:

3.1 Adaptive Filtering

Normally when echo appears adaptive filter is typically been used to overcome the noise whether known or repetition of echo happens. Diagram below shows the basic form of time-domain adaptive filtering application in echo cancellation.

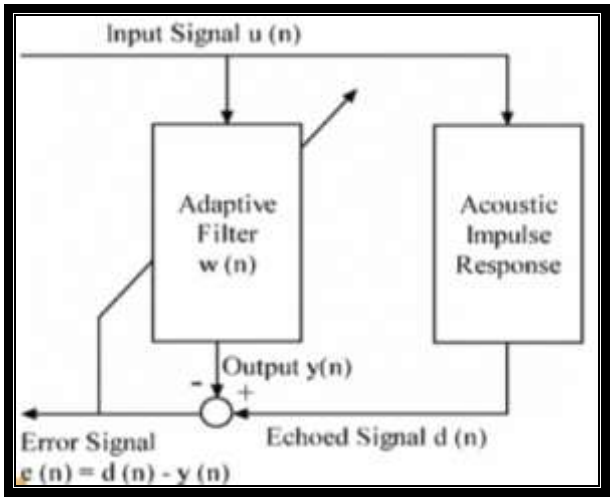

Figure 4: Adaptive Echo Cancellation block diagram

3.2 Principle of Echo Cancellation

The typical ways of echo cancellation are primarily according to the identification of the acoustic channel. This channel is commonly modelled by a finite impulse response (FIR) filter with length This linear modelling could be justified by understanding that the channel is , initially approximation , com posed basically of delay and attenuation . The longer the valuable period assist of the impulse response, the larger is the length L needed for modelling. In practice, this time support can vary from several dozen milliseconds (vehicle compartment) to several hundred milliseconds (conference room).

The echo cancellation algorithm enables filter to be estimated by the L-size vector h(k) using a criterion based on the a priori estimation error. This estimation error, called residual echo, is written, for each sample k.

$$e(k) = y(k) - \mathbf{h}^T(k)\mathbf{x}(k)$$

$$\text{where } \mathbf{x}(k) = [x(k), x(k-1), \ldots, x(k-L+1)]^T$$

The L last samples of the loudspeaker signal. The filter is updated at each instant by feedback of the estimation error proportional to the adaptation gain, denoted as c(k) , and according to

$$\mathbf{h}(k+1) = \mathbf{h}(k) - \mathbf{c}(k)e(k)$$

The different echo cancellation algorithms are distinguished by the gain calculation c(k).These algorithms can be classified as follows

(i) Algorithms produced from the gradient least mean squares in which the optimization criterion correspondents to a reduction of the mean-square error.
(ii) (RLS) Recursive least squares algorithms are depending on a reduction of the criterion of the least squares with exponential forgetting where is a forgetting factor.

$$J[\mathbf{h}(k)] = \sum_{i=0}^{k} \lambda^{k-i} \left[y(i) - \mathbf{h}^T(i)\mathbf{x}(i) \right]^2$$

Moreover, the predictable part of the input signal can be extracted with predictors of lower order than the filter size leading to a class of Newton-type algorithms known as fast Newton transversal filters.

4. ACOUSTIC ECHO CANCELLATION

Block diagram below shows the structure of the AEC adaptive filtering.

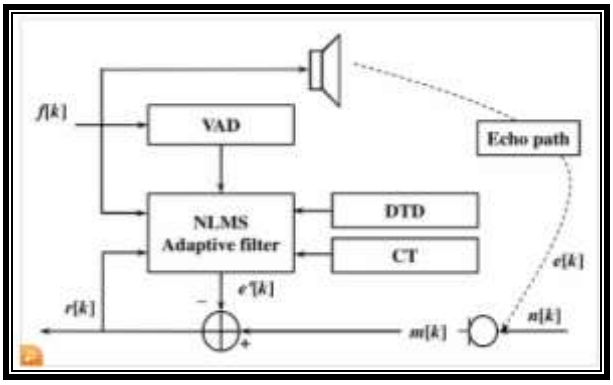

Figure 5: Block Diagram of proposed AEC

A good canceller its performe during the DT it is one of the important characteristics.

$$p[k+1] = (1-\alpha_{high})p[k] + \alpha_{high} f[k]^2 \geq \gamma, \quad p[k] \geq p[k-1]$$

$$p[k+1] = (1-\alpha_{low})p[k] + \alpha_{low} f[k]^2 \geq \gamma, \quad p[k] < p[k-1]$$

In order to overcome the problem of the AEC, a proper methodology to be designed to filter out the Acoustic Echo Cancellation. A flow chat above shows the methodology proposed for the Acoustic Echo Cancellation.

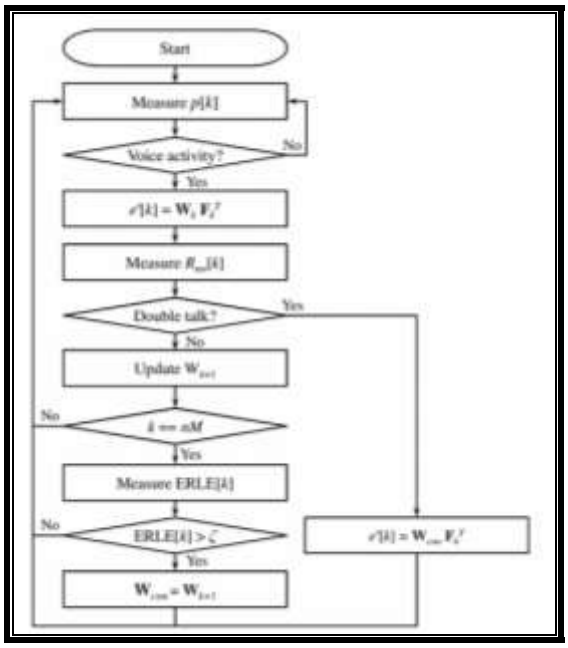

Figure 4 Proposed AEC

4.1 Types of Noise Signals

Five types of common signal that can be interrupted an acoustic environment as shown in table below. By using Acoustic Noise Canceller system all kind of noise able to remove.

Table 1: Varieties of Noise Signal

Types of Noise	Description
Violet	Frequency premphasis 6dB intensity characteristic of f ^2 inverse of brown noise
Blue	Sense of inverse pink noise
Brown	Kind of noise with random walks
Pink	The most prevalent noise in nature
White	Flat response

5. CONCLUSION

In this paper clearly explained the method of Acoustic Echo cancellation specifically chosen to enhance the quality of the conversation especially for hands-free set. Additionally adaptive filter proposed to satisfy the demanded echo reduction furthermore the missed DT was compensate during voice growing time. Implementing the adaptive filter in the frequency domain, on the other hand, reduces the computation complexity and improves the AEC performance. Last but not list the proper methodology been designed to propose the Acoustic echo cancellation.

6. ACKNOWLEDGMENTS

We are grateful to Centre for Telecommunication Research and Innovation (CeTRI) and Universiti Teknikal Malaysia Melaka (UTeM) through PJP/2013/FKEKK (29C)/S01215 for their kind and help for supporting financially and supplying the electronic components and giving their laboratory facility to complete this study.

7. REFERENCES

[1] Halder, Patrashiya Magdolina, and AKM Fazlul Haque. "Improved Echo cancellation in VOIP." Dept. of Electronics and Telecommunication Engineering, Daffodil International University, Dhaka, Bangladesh, International Journal of Advanced Computer Science and Applications 2.11 (2011).

[2] http://www.pikatechnologies.com/english/View.asp?mp=825&x=832

[3] http://www.voipunlimitedcalls.com/the-use-of-voip-echo-cancellation/

[4] http://www.adaptivedigital.com/product/echo_cancel/echo_explain.htm

[5] N. M. Z. Hashim, A. F. Jaafar, Z. Zakaria, A. Salleh, and R. A. Hamzah, "Smart Casing for Desktop Personal Computer," International Journal of Engineering and Computer Science (IJECS), vol. 2, no. 8, pp. 2337–2342, 2013.

[6] N. M. Z. Hashim, N. H. Mohamad, Z. Zakaria, H. Bakri, and F. Sakaguchi, "Development of Tomato Inspection and Grading System using Image Processing," International Journal Of Engineering And Computer Science (IJECS), vol. 2 no. 8, pp. 2319-2326, 2013.

[7] N. M. Z. Hashim, N. A. Ali, A. Salleh, A. S. Ja'afar, and N. A. Z. Abidin, "Development of Optimal Photosensors Based Heart Pulse Detector," International Journal Of Engineering and Technology (IJET), vol. 5, no. 4, pp. 3601–3607, 2013.

[8] N. M. Z. Hashim, N. M. T. N. Ibrahim, Z. Zakaria, F. Syahrial, and H. Bakri, "Development New Press Machine using Programmable Logic Controller," International Journal of Engineering and Computer Science (IJECS), vol. 2, no. 8, pp. 2310–2314, 2013.

[9] N. M. Z. Hashim, N. A. Ibrahim, N. M. Saad, F. Sakaguchi, and Z. Zakaria, "Barcode Recognition System," International Journal of Emerging Trends & Technology in Computer Science (IJETTCS), vol. 2, no. 4, pp. 278–283, 2013.

International Journal of Science and Engineering Applications
Volume 3 Issue 5, 2014, ISSN-2319-7560 (Online)

Design, Simulation and Fabrication of a Microstrip Bandpass Filter

Shreyasi Srivastava
Dept. of Telecommunication
R.V.C.E
Bangalore, India

R.K.Manjunath
Dept. of Instrumentation Sri
Krishna Devaraya University
Anantpur, India

Shanthi P.
Dept. of Telecommunication
R.V.C.E
Bangalore, India

Abstract: This paper presents the design technique, simulation, fabrication and comparison between measured and simulated results of a parallel coupled microstrip BPF. The filter is designed and optimized at 2.44 GHz with a FBW of 3.42%. The first step in designing of this filter is approximated calculation of its lumped component prototype. Admittance inverter is used to transform the lumped component circuit into an equivalent form using microwave structures. After getting the required specifications, the filter structure is realized using parallel coupled technique. Simulation is done using ADS software. Next, optimization is done to achieve low insertion loss and a selective skirt. The simulated filter is fabricated on FR-4 substrate. Comparison between the simulated and measured results shows that they are approximately equal.
Keywords: Advanced Design System (ADS), Flame retardant 4 (FR-4), Bandpass Filter (BPF), Fractional Bandwidth (FBW)

1. INTRODUCTION

The microwave filter is a two port network which is used to control the frequency response at a specific point in a communication system by providing transmission at frequencies within the passband and attenuation in the stopband of a filter. Around the years preceding World War II, microwave filter theory and practice began by pioneers such as Mason, Sykes, Darlington, Fano, Lawson and Richards. Today, most microwave filter designs are done with sophisticated computer-aided design (CAD) packages based on the insertion loss method. The image parameter method may yield a usable filter response for some applications, but there is no methodical way of improving the design. The insertion loss method, however, allows a high degree of control over the passband and stopband amplitude and phase characteristics, with a systematic way to synthesize a desired response[1],[2].

1.1 Bandpass Filter

A bandpass filter only passes the frequencies within a certain desired band and attenuates others signals whose frequencies are either below a lower cutoff frequency or above an upper cut-off frequency. The range of frequencies that a bandpass filter allows to pass through is referred as passband. A typical bandpass filter can be obtained by combining a low-pass filter and a high-pass filter or applying conventional low pass to bandpass transformation.

The ideal bandpass filter has a flat passband where no gain or attenuation is there and all frequencies outside the passband are completely rejected. In general condition, there is no ideal band pass filter. Thus, it can be said that the filters do not attenuate all frequencies outside the desired frequency range. This phenomenon is known as filter roll off and is usually expressed in dB of attenuation per octave or decade of frequency. The resonant series and parallel LC circuits are combined to form a band-pass filter as shown in Fig.1below. In this circuit, the resonant series LC circuits are used to allow only the desired frequency range to pass while the resonant parallel LC circuit is used to attenuate frequencies outside the passband by shunting them towards the ground.

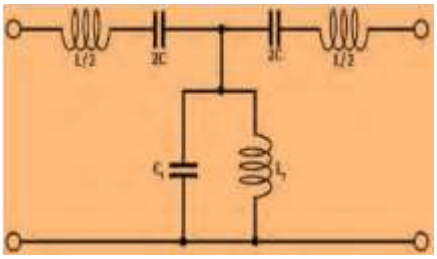

Fig.1 Example of a bandpass filter

Lumped components come with parasitics. For example, an inductor has parasitic resistance and parasitic capacitance. As high frequency is approached (around 1 GHz), parasitics start affecting the frequency response of the filter. It is also very difficult to model a lumped component. Thus, lumped component bandpass filter circuit is converted to microstrip transmission line structure using various methods such as richard's transformation, kuroda's identities, immitance inverters and so on[3].
Nowadays, a microstrip transmission line or strip line is being made as a filter due to its behavior as a good resonator. Micro strip lines give better compromise in terms of size and performance than lumped element filters. The microstrip transmission lines consist of a conductive strip of width (W) and thickness (t) and a wider ground plane, separated by a dielectric layer (ε) of thickness (h) as shown in Fig. 2 below.

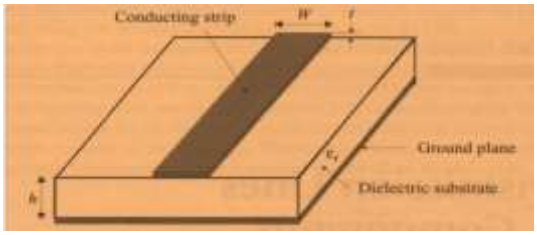

Fig.2 General microstrip structure

1.2 Microstrip

A microstrip line filter type includes stub impedance, step impedance and coupled line filter. Parallel coupled

transmission-line filter in microstrip and stripline technology are very common for implementation of bandpass and band-stop filters with required bandwidth up to a 20 % of central frequency. Due to their relatively weak coupling, this type of filter has narrow fractional bandwidth but instead has desired advantages such as low-cost fabrication, easy integration and simple designing procedure[4]. Designing equations for the coupled line parameters such as space-gap between lines and line widths and lengths, can be found in classical microwave books. This way, following a well-defined systematic procedure, the required microstrip filter parameters can be easily derived for Butterworth and Chebyshev prototypes. The same can be done by using ADS software too.

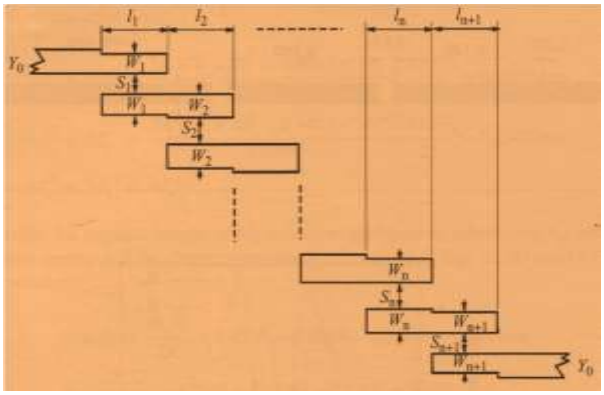

Fig.3 General structure of microstrip parallel coupled line filter

In the figure above, the width, gap, length and impedance are labeled as (W), (S), (l), and (Y0) consequently. The coupling gaps correspond to the admittance inverters in the low-pass prototype circuit(Fig.4). Even- and odd- mode characteristic impedances of parallel-coupled half-wave resonators are computed using admittance inverters. These even- and odd-mode impedances are then used to compute physical dimensions of the filter.

1.3 ADS Software

ADS is used as the simulation software. Advanced Design System (ADS) is an electronic design automation software system produced by AGILENT EEs, a unit of Agilent Technologies. It provides an integrated design environment to designers of RF electronic products such as mobile phones, pagers, wireless networks, satellite communications, radar systems, and high speed data links. Agilent ADS supports every step of the design process—schematic capture, layout, frequency-domain and time-domain circuit simulation, and electromagnetic field simulation—allowing the engineer to fully characterize and optimize an RF design without changing tools.

1.3 FR-4 PCB

Fabrication of the filter is done on FR-4 printed circuit board. FR-4, an abbreviation for Flame Retardant 4, is a type of material used for making a printed circuit board (PCB). It describes the board itself with no copper covering. The FR-4 used in PCBs is typically UV stabilized with a tetra functional epoxy resin system. It is typically a yellowish color. FR-4 manufactured strictly as an insulator (without copper cladding) is typically a dysfunctional epoxy resin system and a greenish color. FR-4 is preferred over cheaper alternatives such as synthetic resin bonded paper (SRBP) due to several mechanical and electrical properties; it is less loss at high frequencies, absorbs less moisture, has greater strength and stiffness and is highly flame resistant compared to its less costly counterpart. Fr-4 is widely used to build high-end consumer, industrial, and military electronic equipment. It is also ultra-high vacuum (UHV) compatible[5].

2. DESIGN FLOW

A chebyshev filter is designed to operate between 2.40-2.48 GHz with the center frequency of 2.44 GHz[6]. Passband ripple is taken as 0.5 dB. Insertion loss and return loss are required to be ≤ 1 dB and > 15 dB respectively.

The first step in designing a filter is to find its order. The fractional bandwidth and normalized frequency are found by the formulae given below[7].

$$\text{Fractional Bandwidth (FBW)} = \frac{\omega 2 - \omega 1}{\omega o} = 0.0342$$

$$\text{Normalized Frequency} = \left| \frac{\omega}{\omega 1} \right| - 1 = 0.42$$

Here, ω1 and ω2 are the edge frequencies and ωo is the center frequency. Then the order of the filter is found out by the attenuation $v_{s.}$ normalized frequency graph for 0.5 dB ripple as shown in the graph given below.

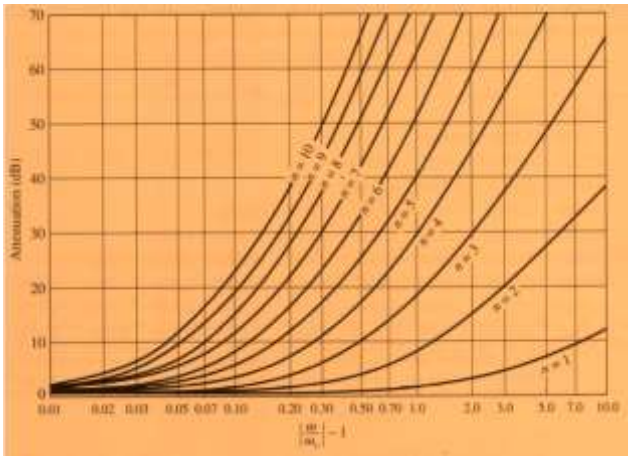

Graph 1. Attenuation $v_{s.}$ normalized frequency graph for 0.5 dB

The order of the filter is n=5 at minimum attenuation=20dB and normalized frequency=0.42. The element values for fifth order filter are determined from Table 1.

Table 1. Table of Element values for 0.5dB ripple low pass filter prototype

0.5 dB Ripple										
N	g_1	g_2	g_3	g_4	g_5	g_6	g_7	g_8	g_9	g_{10}	g_{11}
1	0.6986	1.0000									
2	1.4029	0.7071	1.9841								
3	1.5963	1.0967	1.5963	1.0000							
4	1.6703	1.1926	2.3661	0.8419	1.9841						
5	1.7058	1.2296	2.5408	1.2296	1.7058	1.0000					
6	1.7254	1.2479	2.6064	1.3137	2.4758	0.8696	1.9841				
7	1.7372	1.2583	2.6381	1.3444	2.6381	1.2583	1.7372	1.0000			
8	1.7451	1.2647	2.6564	1.3590	2.6964	1.3389	2.5093	0.8796	1.9841		
9	1.7504	1.2690	2.6678	1.3673	2.7239	1.3673	2.6678	1.2690	1.7504	1.0000	
10	1.7543	1.2721	2.6754	1.3725	2.7392	1.3806	2.7231	1.3485	2.5239	0.8842	1.9841

The element values obtained are: g1 =g5 =1.7058, g2 =g4=1.2296, g3=2.5408. The low-pass prototype elements values obtained can be represented as shown in Figure 4.

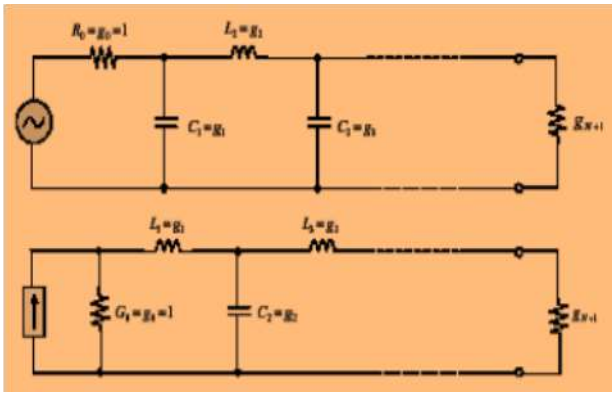

Fig. 4 Low pass filter prototype

The low-pass filter consists of series and parallel branch. J-inverter is used to convert low-pass filter to bandpass filter with only shunt branch as shown in figure 5.

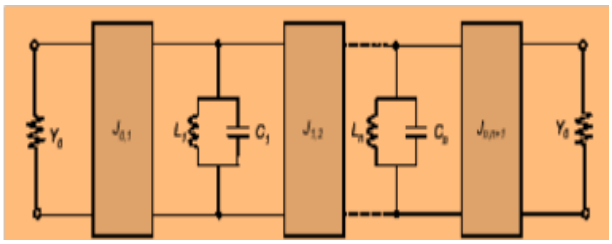

Fig. 5 Bandpass filter prototype

Using the equations given below, J-inverter performs the low pass to bandpass conversion.

$$\frac{J_{0,1}}{Y_0} = \sqrt{\frac{\pi FBW}{2 g_0 g_1}}$$

$$\frac{J_{j,j+1}}{Y_0} = \frac{\pi FBW}{2\sqrt{g_j g_{j+1}}}$$

---------j=1 to n-1

Where FBW is the fractional bandwidth of the bandpass filter, Jj, j+1 are the characteristic admittances of the J-inverters and Y_0 the characteristic admittance of the terminating lines. To realize the J-inverters, even- and odd-mode characteristic impedances of coupled lines are determined by using the relations given below.

$$(Z_{0e})_{j,j+1} = \frac{1}{Y_0}\left[1 + \frac{J_{j,j+1}}{Y_0} + \left(\frac{J_{j,j+1}}{Y_0}\right)^2\right]$$

$$(Z_{0o})_{j,j+1} = \frac{1}{Y_0}\left[1 - \frac{J_{j,j+1}}{Y_0} + \left(\frac{J_{j,j+1}}{Y_0}\right)^2\right]$$

-------j=0 to n

The calculated results are tabulated below.

Table 2. Parallel coupled filer parameters

Stages of filter	Admittance inverters $J_{j,j+1}/Y_0$	Even mode impedance (Z_{0e})	Odd mode impedance(Z_{0o})
1	0.17746	60.4476	42.7016
2	0.03709	51.923	48.214
3	0.03039	51.5656	48.5266
4	0.03039	51.5656	48.5266
5	0.03709	51.923	48.214

By using the LineCalc tool in Advanced Design System (ADS), Agilent Technologies version 2013 software, the dimensions of width, spacing and length of each stage are calculated by using even and odd characteristic impedance. The characteristic impedance Z_0 is typically assumed as 50 Ohms. The standard FR-4 board requirements are-

Table 3 FR-4 Specifications

Conductor thickness	0.035mm
Height	1.6mm
ε_R	4.8
tanδ	0.002
conductor conductivity	5.8e7

Next, optimization is done. All parameters and goals have to be set up properly. After that, the optimization and tuning process carried on for the best results and performance. The finalized dimensions of width, gap and length of each stage are shown in Table 4 below.

Table 4 Geometrical parameters of the coupled lines

Line description	Width(mm)	Length(mm)	Spacing(mm)
50Ω-line1	2.61	4.1137	-
Coupled line1	2.61	11.704	0.35261
Coupled line2	2.61	19.3057	3.558
Coupled line3	2.61	11.727	0.473
Coupled line4	2.61	11.41799	0.11089
Coupled line5	2.61	19.255	0.498
50Ω-line2	2.61	4.35312	-

3. IMPLEMENTATION IN ADS

As a final step, the coupled line filter is designed in the ADS simulation software environment. It accepts filter parameters and produces physical dimensions of the filter layout and a simulation of the filter response.

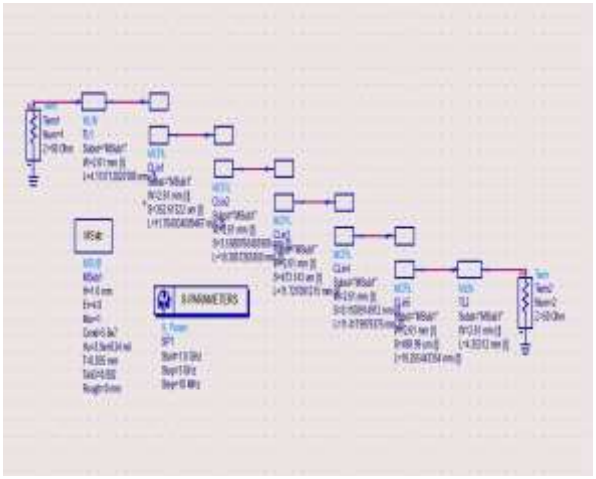

Fig. 6 Schematic of parallel coupled bandpass filter

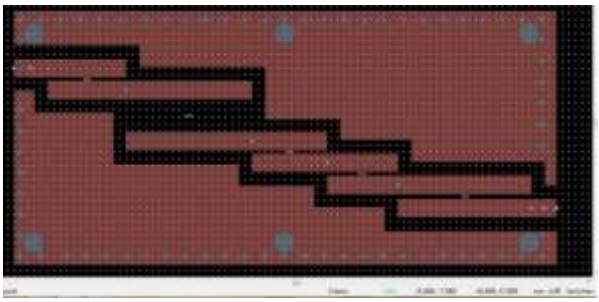

Fig. 7 PCB Layout of parallel coupled bandpass filter

3.1 Simulation

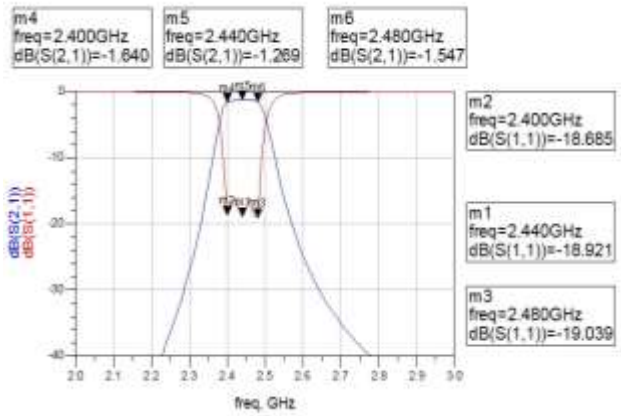

Fig. 8 Simulation result of parallel coupled band pass filter for S (1, 1) and S (2, 1)

Table 5 Simulation results

Parameter	Lower Frequency(ω1) 2.40 GHz	Upper Frequency(ω2) 2.48 GHz	Center Frequency(ω_0) 2.44 GHz
S(1,1)	-18.685 dB	-19.039 dB	-18.685 dB
S(2,1)	-1.640 dB	-1.547 dB	-1.269 dB

The calculated bandwidth was 80MHz.The Simulated bandwidth is less than the calculated bandwidth. The specified insertion loss was supposed to be less than or equal to 1dB but the simulated insertion loss is between 1 to 2 dB. The simulated passband ripple is less than 1dB as per the specifications. The return loss is greater than 15dB as required.

4. FABRICATION

Filter PCB is fabricated using FR-4 board. Filter lay out was generated in ADS tool in Gerber format. It can be noticed from Fig 8 that many plated through holes are made all around the filter to nullify the parasitic effects. Mounting holes are also through drilled and through hole plated at appropriate distances to provide good grounding. Finally the Filter PCB is mounted inside a mechanical housing which is fabricated using Aluminum strips/blocks. Finally the whole housing was CCC plated for better electrical performance SMA connectors are mounted on to the housing in such a way that the center pin of the SMA connector directly land on to the 50 Ohms line for Input/out connectivity.

Fig. 8 Fabricated microstrip parallel coupled line band pass filter

5. TESTING

Performance of the Filter is tested using R&S Scalar Network Analyzer ZLV13, which is 13 GHz network Analyzer[8]. Fig 9 shows the test set up. Transmission measurements were carried out using S12/S21 set up and Reflection/Return Loss measurements were carried out with S11 and S22 set up

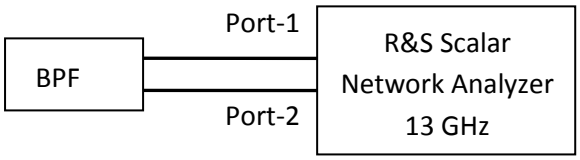

Fig. 9 Test set up for testing micro strip parallel coupled line band pass filter

Table 6 Tested results

Parameter	Lower Frequency(ω1) 2.40 GHz	Upper Frequency(ω2) 2.48 GHz	Center Frequency(ω_0) 2.44 GHz
S(1,1)	-16.5dB	-16 .1dB	-17.3 dB
S(2,1)	-3.0 dB	-3.1dB	-2.7dB

6. CONCLUSION

It can be seen from the test results that insertion loss figures are slightly more (1.5 dB) than the simulated test results.

This may be due to Fabrication anomalies/mistakes.FR4 material losses and dielectric unevenness's may also be the reasons for higher insertion loss. It is definitely possible to achieve better results using Teflon Board instead of FR4.

7. REFERENCES

[1] I. Azad, Md. A. H. Bhuiyan, S. M. Y. Mahbub, "Design and Performance Analysis of 2.45 GHz Microwave Bandpass Filter with Reduced Harmonics", International Journal of Engineering Research and Development, vol. 5, no. 11, pp. 57-67, 2013.

[2] Jia-Sheng Hong, "Microstrip Filter for RF/Microwave Application", John Willey and Sons, Inc, Second edition, pp. 112 160, 2011.

[3] M. Alaydrus, *Transmission Lines in Telecommunication*, Graha Ilmu Press, Jogjakarta, 2009 (in Indonesian).

[4] C. Wang and K A. Zaki, "Dielectric resonators and filters," *IEEE Microwave Magazine*, vol. 8, no. 5, pp. 115-127, Oct. 2007.

[5] R. V. Snyder, "Practical aspects of microwave filter development," *IEEE Microwave Magazine*, vol. 8, no. 2, pp. 42-54, Apr. 2007.

[6] S. Seghier, N. Benahmed, F. T. Bendimerad, N. Benabdallah, "Design of parallel coupled microstrip bandpass filter for FM Wireless applications", Sciences of Electronics, Technologies of Information and Telecommunications (SETIT), 6th International Conference, pp. 207-211,21-24 March 2012.

[7] M. Kirschning and R.H. Jansen, "Accurate wide-range design equations for the frequency-dependent characteristic of parallel coupled microstrip lines," *IEEE Transactions on Microwave Theory and Techniques*, vol. 32, no. 1, pp. 83-90, Jan.1984.

[8] P. W. Wong and I. Hunter, "Electronically tunable filters," *IEEE Microwave Magazine*, vol. 10, no. 6, pp. 46-54, Oct. 2009.

[9] O.A.R. Ibrahim, I.M. Selamat, M. Samingan, M. Aziz, A. Halim, "5.75 GHz microstrip bandpass filter for ISM band," in proc. of *Applied Electromagnetics, 2007 Asia-Pacific Conf. on*, pp. 1-5, Dec. 2007.